1 # Antibiotics select for novel pathways of resistance in biofilms

2

3

4 Eleftheria Trampari[1], Emma R Holden[1], Gregory J Wickham[1], Anuradha Ravi[1],

5 Filippo Prischi[3], Leonardo de Oliveira Martins[1], George M Savva[1], Vassiliy N. Bavro[3],

6 Mark A Webber[1,2*]

7

8

9 [1]Quadram Institute Bioscience, Norwich Research Park, Norwich, Norfolk, NR4 7UQ,

10 U.K.

11 [2]Medical School, University of East Anglia, Norwich Research Park, Norwich,

12 Norfolk, NR4 7UA, U.K.

13 [3]School of Biological Sciences, University of Essex, Wivenhoe Park, Colchester,

14 CO4 3SQ, U.K.

15

16

17 *mark.webber@quadram.ac.uk +

18

Abstract

Most bacteria in nature exist in aggregated communities known as biofilms. Bacteria within biofilms are inherently highly resistant to antibiotics. Current understanding of the evolution and mechanisms of antibiotic resistance is largely derived from work from cells in liquid culture and it is unclear whether biofilms adapt and evolve in response to sub-inhibitory concentrations of drugs. Here we used a biofilm evolution model to show that biofilms of a model food borne pathogen, *Salmonella* Typhimurium rapidly evolve in response to exposure to three clinically important antibiotics. Whilst the model strongly selected for improved biofilm formation in the absence of any drug, once antibiotics were introduced the need to adapt to the drug was more important than the selection for improved biofilm formation. Adaptation to antibiotic stress imposed a marked cost in biofilm formation, particularly evident for populations exposed to cefotaxime and azithromycin. We identified distinct resistance phenotypes in biofilms compared to corresponding planktonic control cultures and characterised new mechanisms of resistance to cefotaxime and azithromycin. Novel substitutions within the multidrug efflux transporter, AcrB were identified and validated as impacting drug export as well as changes in regulators of this efflux system. There were clear fitness costs identified and associated with different evolutionary trajectories. Our results demonstrate that biofilms adapt rapidly to low concentrations of antibiotics and the mechanisms of adaptation are novel. This work will be a starting point for studies to further examine biofilm specific pathways of adaptation which inform future antibiotic use.

43 **Main**

44 Antimicrobial resistance (AMR) is a complex problem and is a major threat to human

45 and animal health (1). Understanding how bacteria develop resistance to antibiotics

46 is important to inform how they should be used to minimise selection of AMR. There

47 are many genetic mechanisms of antibiotic resistance and the selection of resistant

48 mutants is a classic example of natural selection (2). Initial studies of mechanisms of

49 resistance tended to expose populations to very high concentrations of antibiotics

50 and select for survivors. This identified 'high-impact' mutations can confer a large

51 phenotypic benefit and proved very useful for characterising cellular targets and

52 primary resistance mechanisms. However, more recent work has found that

53 repeated exposure to sub-inhibitory concentrations of antimicrobials can have

54 profound impacts on bacterial populations including selection for high level

55 resistance (3,4). This better reflects real world situations where low levels of

56 antimicrobials are commonly present. Importantly, this allows epistatic interactions

57 between multiple genes to be selected and for fitness costs arising from resistance

58 mutations to be ameliorated by additional, compensatory mutations (5).

59 Much of our understanding of the mechanisms of antibiotic action and resistance

60 comes from laboratory experiments in which bacteria are routinely grown in liquid

61 culture before being exposed to antibiotics. Yet most bacteria in nature exist in

62 biofilms; aggregates of cells often attached to a surface (6). Biofilms represent a

63 fundamentally different mode of life to planktonic cultures and multiple studies have

64 demonstrated extreme changes in gene and protein expression profiles from the

65 same strains when grown in liquid or as a biofilm (7). Many infections include a

66 biofilm component which makes the infection difficult to treat; common examples

67 include infections on prosthetic or indwelling devices. One of the hallmarks of

3

68   biofilms is inherit resistance to antibiotics, when compared to the corresponding

69   strain grown in liquid culture. One theory explaining the high degree of resistance to

70   antibiotics in biofilms is that cells within a biofilm are metabolically inactive, or even

71   'persisters'. In these dormant subpopulations, characterised by arrested

72   macromolecular syntheses, the cellular targets which the antibiotics poison are not

73   essential, thus impeding the bactericidal activity of the antibiotic (8). However, recent

74   studies have demonstrated a strong evolutionary pressure for strains to evolve

75   improved biofilms. In particular, rapid selection of mutants and combinations of

76   mutants with improved biofilm fitness is observed when bacteria are introduced to a

77   new niche (9–11).

78   Given this evidence of adaptation within biofilms we were interested whether

79   exposure to low concentrations of antibiotics would exert a selective effect on cells

80   within a biofilm. We hypothesised that exposure of biofilms to sub-lethal

81   concentrations of antibiotics would impart a selective pressure and the outcomes of

82   this stress would be distinct to those seen in planktonic cells. To test this hypothesis,

83   we adapted an experimental biofilm evolution model and used *Salmonella*

84   Typhimurium as a model biofilm-forming pathogen which we exposed to three

85   clinically relevant antibiotics. We compared drug exposed biofilm lineages to

86   unexposed biofilm controls and exposed planktonic lineages. We measured the

87   emergence of antibiotic resistance, biofilm capacity, and pathogenicity, and

88   subsequently investigated condition-specific mechanisms of resistance using

89   genome sequencing. We observed rapid adaptation to antibiotic pressure which

90   often carried a cost for biofilm formation, identified novel mechanisms of resistance

91   against cefotaxime and azithromycin and detected biofilm-specific phenotypes

4

92 showing that studying how biofilms adapt to stress is vital to understanding the

93 evolution of AMR.

Results

95 **A biofilm evolution model can study responses to antimicrobial stress**

96 To study the evolution and adaptation of *S.* Typhimurium biofilms when exposed to

97 antibiotics, a serial transfer bead-based model system was adapted and optimised

98 (based on previous work by the Cooper group (11)). To establish *Salmonella*

99 biofilms, we grew bacteria on glass beads in broth (see materials and methods). The

100 beads served as a substrate for biofilms to form on and as a biofilm transfer vehicle,

101 used to move mature biofilms to new tubes with fresh media and new sterile beads.

102 After each transfer, bacteria from the biofilm community had to colonise the new

103 beads and establish biofilms on their surface before being transferred again. This

104 system allows repeated longitudinal exposure of biofilms to the stress of interest and

105 captures all the major components of the biofilm lifecycle. After each passage, cells

106 from biofilms were harvested and populations and individual representative strains

107 were stored and phenotypically characterised. Strains that developed resistance or

108 exhibited altered biofilm formation were selected for whole-genome-sequencing to

109 identify the genetic basis of these phenotypes (Figure 1, a-d).

110 To determine the appropriate conditions for the evolution experiments, we measured

111 biofilm formation by *S.* Typhimurium 14028S in lysogeny broth (without salt) after 24,

112 48, 72 and 96 hours, at 25°C, 30°C, 37°C and 40°C respectively (Figure 1, e). Biofilm

113 formation was determined by measuring cfu per bead (Figure 1, e). Over 72 hours

114 the highest amount of biomass formed (~10^6 cfu/ bead) was after incubation at 25°C

5

115   or 30ºC; this was stable and consistent. Therefore, we ran the evolution experiments

116   at 30ºC with a passage period of 72 hours.

117   To investigate if and how biofilms would adapt to exposure to sub-inhibitory

118   concentrations of antibiotics, we grew biofilms on beads, in the presence of three

119   clinically-important antibiotics for the treatment of Salmonellosis; azithromycin,

120   cefotaxime and ciprofloxacin. The minimum inhibitory concentrations (MICs) for each

121   antibiotic were determined following the EUCAST microbroth dilution method,

122   adapted to use LB-NaCl and 30 °C to replicate the experimental conditions. Growth

123   kinetics in the presence of all three agents were determined at the same conditions.

124   Based on these results we identified concentrations of each agent (10 µg/mL

125   azithromycin, 0.062 µg/mL cefotaxime and 0.015 µg/mL of ciprofloxacin) that reliably

126   restricted planktonic growth rates to approximately 50% of that of unstressed control

127   cultures which were then used for evolution experiments. This approach had proved

128   tractable in our previous planktonic evolution experiments with biocides (12).

129   We ran three separate evolution experiments, one with each antibiotic. Within each

130   we included eight lineages; four exposed bead lineages, two exposed planktonic

131   cultures and two drug-free bead-control lineages (Figure 1b). Populations from early,

132   middle and late time points of each experiment were harvested from beads and three

133   single colonies were isolated to allow us to examine phenotypic diversity within the

134   population. The isolates were tested for their biofilm ability, morphology and

135   susceptibility. Biofilm formation was monitored using the Crystal Violet assay (CV)

136   assay and matrix production assessed qualitatively by visualising colonies grown on

137   Congo Red (CR) plates. Susceptibility to antibiotics was measured by determining

138   MICs using the agar dilution method (13).

139   To confirm the model selects for evolution of increased biofilm formation we

140   phenotyped isolated single cells from drug-free bead-control lineages. We observed

141   an incremental increase in biofilm formation with unexposed isolated colonies

142   forming larger and wrinklier biofilms on CR plates and producing more than three

143   times as much biomass over the course of the experiment (Figure 1, f). This

144   confirmed the model strongly selects for adaptation to produce biofilms with

145   increased biomass over time in the absence of any stressor.

146   **Biofilms rapidly evolve and adapt in response to sub-inhibitory antibiotic**

147   **concentrations**

148   To test the phenotypic responses of biofilms repeatedly exposed to non-lethal

149   concentrations of the test antibiotics, we isolated both populations and three

150   individual strains from each lineage at three different timepoints of all experiments;

151   early (first passage), mid (half way point) and late (final passage). We characterised

152   these populations as well as isolated strains for susceptibility to eight clinically-

153   relevant antimicrobials, biofilm formation and colony morphology. We compared

154   results from the biofilm lineages with the corresponding planktonic lineages run at

155   the same time (Figure 2).

156   Biofilms rapidly evolved resistance in response to all three exposures (Figure 2). The

157   time taken to select for emergence of mutants with decreased susceptibility to the

158   antibiotics was similar in both biofilm and planktonic lineages. Azithromycin selected

159   mutants in a stepwise manner with emergence of a population with an 8-fold MIC

160   increase, followed by selection of highly resistant populations with MICs of

161   azithromycin 16 times more than the parent strain. The decreased susceptibility of

162   the azithromycin-exposed lineages became evident at the earliest time point and

163   was fixed by the mid-point of the experiment (Figure 2 a, b). Cefotaxime

164 demonstrated a similar dynamic with both planktonic populations and biofilms

165 exhibiting decreased susceptibility and maintaining this resistance profile until the

166 end of the experiment (Figure 2, c-d). Adaptation to ciprofloxacin resistance was

167 selected by the middle of the experimental period and remained fixed up to the final

168 timepoint in both biofilm and planktonic lineages (Figure 2 e, f).

169 While the selection dynamics seemed similar between biofilm and planktonic

170 lineages at first glance, analysis of the MICs to all the antibiotics tested, revealed

171 significant differences in the outcomes between biofilm and planktonic conditions.

172 For instance, whilst planktonic populations, exposed to cefotaxime, become mainly

173 resistant to cefotaxime, cefotaxime-exposed biofilms exhibited a multidrug resistance

174 (MDR) phenotype (Figure 2, d). These observations show that whilst the biofilms are

175 able to develop resistance to the selective antibiotics, the mechanisms are likely to

176 be distinct to those seen in planktonic culture.

177 Whilst it is widely accepted that increased biomass and matrix production improves

178 resilience of biofilms to antimicrobial stress, we observed that biofilm formation itself

179 is heavily influenced by the selective antibiotic. For example, azithromycin prevented

180 the strains from adapting and forming better biofilms whereas unexposed biofilms

181 produced much more biomass over time (Figure 2b). Cefotaxime had a strong

182 negative effect on biofilm formation, with biofilms exposed to cefotaxime actually

183 producing less biomass than the starting wild-type strain and being characterised by

184 pale colony morphology on CR plates (Figure 2d). Ciprofloxacin had less impact on

185 biofilm formation and biofilms exposed to this drug produced increased biomass over

186 time, although to only half the level of the control biofilms. As expected, isolates from

187 planktonic lineages did not form better biofilms over time. On the contrary,

188   cefotaxime exposure again selected for weaker biofilms with a pale colony

189   morphology on CR plates (Figure 2c).

190   **Individual antibiotics select specific pathways to resistance in biofilms**

191   To investigate correlations between development of resistance to different antibiotics

192   and biofilm formation after each exposure, we compared fold changes in MIC of

193   antibiotics with fold changes in biofilm formation (Figure 3). Each point on the graphs

194   represents a single isolated strain from each evolution experiment (blue:

195   azithromycin exposure, white: cefotaxime exposure, red: cipro exposure, black: drug

196   free exposed controls). All results were compared to averaged data from the parent

197   strain (represented as point '0,0' on the graphs).

198   As expected, strains became resistant to the antibiotic they were exposed to. There

199   were also examples of selection of cross-resistance to other antibiotics in the

200   biofilms. For instance, azithromycin-exposed isolates exhibited an MDR phenotype

201   and demonstrated decreased susceptibility not only to azithromycin, but also to

202   cefotaxime, chloramphenicol, ciprofloxacin, nalidixic acid, tetracycline and triclosan.

203   Similarly, the cefotaxime-exposed lineages showed increased MICs of

204   chloramphenicol and tetracycline. Most of the antimicrobials tested are known

205   substrates of multidrug efflux pumps (e.g. AcrAB-TolC) except for kanamycin.

206   Strikingly, this was the only antibiotic to which no cross-resistance was observed. In

207   fact, cefotaxime exposed isolates became more susceptible to kanamycin than the

208   parent strains.

209   Apart from impacts on antibiotic resistance, antibiotic exposure also resulted in major

210   changes in the strains' ability to form biofilms. Bacteria exposed to cefotaxime

211   exhibited severely compromised biofilm ability, whereas azithromycin and

9

212   ciprofloxacin led to inhibition or delayed biofilm adaptation respectively. This analysis

213   again indicates that exposure to antibiotics prompts selection for resistance even at

214   sub-inhibitory concentrations, but that this comes at a cost to the ability to form

215   biofilms.

216   To identify the mechanisms responsible for the phenotypes described above, we

217   whole-genome sequenced over 100 strains (selected to represent major phenotypes

218   of interest and to cover different times in the exposure series for each drug) and

219   identified changes against the parent strain genome. We sequenced a mixture of

220   populations and single cells and used data from single-cell strains to analyse the

221   phylogeny of the mutants (Figure 4a). The results indicated that the different

222   antibiotics selected for mutants which followed distinct paths of adaptation. There

223   was little commonality between the drug exposures showing that there is no

224   universal or generic mechanism of resistance selected for in biofilms. Biofilms

225   exposed to azithromycin and cefotaxime followed a reproducible and distinct

226   evolution pattern (Figure 4b, c), whereas in the ciprofloxacin exposure, bacteria

227   responded to the stress in a number of different ways (Figure 4d). For all drugs,

228   there was separation of biofilm (darker coloured dots) and planktonic lineages

229   (lighter coloured dots) apparent in the phylogeny, again demonstrating different

230   trajectories of selection.

10

231 **Azithromycin and cefotaxime select novel mechanisms of resistance based**

232 **upon exclusion of drug from target which in turn hinders biofilm formation**

233 We used the whole-genome sequencing data to identify mutations which may

234 account for potential mechanisms of resistance against the antibiotics of interest.

235 These include some known mechanisms of resistance (e.g. *gyrA* mutation renders

236 bacteria resistant to quinolones (14–16)), as well as Single Nucleotide

237 Polymorphisms (SNPs) that have never been linked to antimicrobial resistance

238 before. The sequence data gave us enough information to build solid hypotheses

239 about the genetic basis for novel mechanisms of resistance against cefotaxime and

240 azithromycin, which we then tested experimentally using a combination of assays

241 (Figure 5).

242 *Novel mechanisms of cefotaxime resistance*

243 We first observed that isolates that became resistant to cefotaxime had two unique

244 substitutions that they acquired at different timepoints during the evolution

245 experiment. The first substitution was in EnvZ (corresponding to arginine 397 to

246 histidine) and the second was in AcrB (glutamine 176 to lysine).

247 EnvZ is an osmolarity-sensor protein, attached to the inner membrane of the cell. It

248 functions both as a histidine kinase and a phosphatase, exerting its activity by

249 altering the phosphorylation levels of its cognate transcriptional regulator OmpR.

250 OmpR, amongst other functions, is responsible for differential regulation of the

251 expression of OmpC and OmpF, two principal outer-membrane porins (17,18), as

252 well as curli biosynthesis through the *csgD-csgBAC* operon (19). Mutants carrying

253 the substitution of R397H in EnvZ exhibited a 4-fold increase in the MIC of

254 cefotaxime (Figure 5a) of cefotaxime and produced pale colonies on CR plates. This

11

255 substitution was present in both planktonic cultures and in biofilms. It is well

256 established that β-lactams cross the outer membrane via porin channels and

257 particularly through OmpF (20–22). It is also well known that OmpR stimulates curli

258 biogenesis by promoting expression of CsgD, which in turn activates the curli operon

259 (23).

260 AcrB is a key component of the tripartite multidrug efflux pump AcrAB-TolC, and is

261 responsible for substrate recognition and energy transduction (24–26) during the

262 efflux process. Being a member of the *R*esistance *N*odulation cell *D*ivision (RND)

263 family, AcrB shares a common structural organisation with other RND pumps, and

264 couples inward proton transport to antiport (efflux) of a wide range of xenobiotic

265 agents including antibiotics, thus contributing to the emergence of MDR bacteria.

266 The identified Q176K substitution in AcrB was found in strains already containing the

267 EnvZ substitution and led to an additional 4-fold increase in the MIC of cefotaxime

268 (Figure 5a). This substitution was only detected from planktonic cultures and had no

269 additional impact on biofilm formation over that of the EnvZ R397H mutant.

270 Based on the above, we hypothesised that the 'first-step' changes in MIC were due

271 to alterations in expression of *ompC* and *ompF* following mutation of *envZ*.

272 Subsequent substitution in AcrB, was responsible for altered coordination of

273 cefotaxime by AcrB (Q176 is in the distal drug binding pocket of AcrB) and

274 correspondingly lowered residence time of the antibiotic in the pocket, leading to

275 increased efflux of this substrate. Changes in curli expression (due to loss of EnvZ-

276 mediated activation of OmpR), would account for the compromised biofilm formation

277 phenotype we observed for these isolates.

12

278   We tested this hypothesis in a number of ways. First, we isolated RNA from 48-hour

279   biofilms, grown in LB agar plates with no salt, formed by strains carrying the

280   identified substitutions (cef-biofilm-M-D-S1 (EnvZ R397H) and cef-plank-L-S2 (EnvZ

281   R397H/ AcrB Q176H)), as well as the WT strain as a control. We performed qRT-

282   PCR to measure *ompC* and *ompF* expression, using *gyrB* expression as our

283   reference (Figure 5b). We observed a significant reduction in *ompF* expression in

284   both the mutants as well as an overexpression of *ompC* indicating that the balance

285   of porin expression had been altered as predicted (Figure 5b). To test whether the

286   decrease in *ompF* led to reduced drug accumulation in the cells, we used a resazurin

287   drug accumulation assay which confirmed that, both mutants show reduced

288   accumulation of drugs inside the cell (Figure 5d).

289   Additionally, we measured expression of the main curli subunits, *csgA* and *csgB,* and

290   found that expression in the mutants was completely lost (Figure 5c). This explains

291   the pale phenotype on CR and supports our hypothesis that loss of EnvZ function

292   confers protection against cefotaxime, but at a cost to biofilm formation.

293   We confirmed the specific phenotypic impacts of the two substitutions by creating

294   mutants of the parent strain lacking *acrB* or *envZ* and complementing these with

295   either wild-type or mutant alleles and determining the impacts on phenotypes (Figure

296   5a). Deletion of *envZ* and complementation with the WT allele did not lead to any

297   MIC changes for any of the antibiotics tested. However, complementation with the

298   mutant pEnvZ R397H allele led to a significant increase in MICs of cefotaxime,

299   chloramphenicol and tetracycline. Similarly, although complementation of the AcrB

300   deletion strain with AcrB or AcrB Q176K did not have an impact on resistance,

301   complementation of AcrB in a ΔAcrB/ ΔRamR background with the Q176K allele led

302   to decreased susceptibility to cefotaxime, chloramphenicol and tetracycline,

13

303 replicating the phenotype of strains derived from the evolution experiments. These

304 results confirm that the mutations identified are responsible for the resistance

305 phenotypes observed after exposure to cefotaxime.

306 Finally, we performed *in silico* modelling work to investigate the potential impact of

307 the Q176K substitution on AcrB structure and substrate binding (Figure 4e-f).

308 AutoDock VINA docking simulations were used, allowing for flexible side-chains.

309 Analysis of cefotaxime docking, as well as docking of the control antibiotics,

310 nitrocefin and cephalothin, to both the WT (Q176) and the mutant (Q176K), were

311 based on experimental crystallographic studies (supplementary figure S1, a-b). The

312 analysis focused on the distal binding pocket of chain B of AcrB from *E.coli*

313 (4DX5.pdb) (27) corresponding to the "bound" or "tight" protomer conformation. We

314 found that in both cases, Q176 and the mutant side chain, Q176K, participated in the

315 coordination of cephalosporin molecules. However, the coordination was markedly

316 different, between the WT and the mutant, and resulted in statistically significant

317 reduction in the free energy of binding (ΔG) (Supplementary table S1). This supports

318 the idea that the substitution might cause a reduction in the residence time for drugs

319 in the pocket and as a result, increased efflux and decreased susceptibility.

320 *Novel mechanisms of azithromycin resistance*

321 Lineages exposed to azithromycin developed an 8-fold increase in azithromycin MIC

322 (reaching the proposed epidemiological cut-off to define resistance in *Salmonella*

323 (28)) before adapting further to have an MIC 16x higher than the parent (Figure 5f).

324 When we sequenced the resistant strains, we identified two distinct amino acid

325 substitutions. In the first population, there was an arginine 717 substitution to leucine

14

326   in AcrB and the mutants with highest MICs also had a threonine 18 substitution to

327   proline in RamR.

328   Interestingly, this substitution in AcrB is distinct from that observed after cefotaxime

329   exposure, and in a different part of the protein. The distal binding pocket is predicted

330   to control access of substrates into the pump, as well as participating in the

331   coordination of high-molecular mass substrates, such as macrolides in the proximal

332   binding pocket (29,30). This indicates that changes in different parts of AcrB confer

333   resistance to different substrates.

334   RamR is the transcriptional repressor of *ramA*, which is a global transcriptional

335   activator that positively regulates the AcrAB-TolC pump production (31). The

336   inactivation of *ramR* results in over-expression of RamA, consequently increasing

337   pump expression and inducing an MDR phenotype (32). We observed that isolates

338   with this substitution also acquired cross-resistance to cefotaxime, chloramphenicol,

339   nalidixic acid, tetracycline and triclosan, all of which are AcrB substrates.

340   Our hypothesis was that the R717L substitution in AcrB would result in increased

341   efficiency of efflux of azithromycin and as a result, increased resistance. The

342   additional RamR substitution would then result in over-expression of this mutant

343   pump and explain the further increase in the MIC of azithromycin. To test this

344   hypothesis, we extracted RNA from 48-hour old biofilms and we measured

345   expression of *acrB* and *ramA* by q-RT-PCR, again using *gyrB* expression as our

346   reference (Figure 5g). For both targets there was up-regulation in the mutants

347   compared to the parent strain although expression levels of *acrB* in all cells were

348   low; AcrB is primarily produced in growing cells so low levels of *acrB* mRNA was not

349   unexpected. Intracellular drug accumulation was monitored as described above

350   using the resazurin method (Figure 5h). The R717L mutant alone did not show any

351   changes in accumulation compared to the WT, suggesting the substitution does not

352   impact export of this substrate. This supports the idea that this change improves

353   access for larger substrates to the pump (such as azithromycin, Mr:749), which relies

354   on the proximal drug binding vetting. However, this would not impact a small

355   molecule like resazurin (Mr:229), which has been suggested to directly access the

356   distal binding pocket, by bypassing the proximal pocket of the pump (30,33).

357   Consistent with this idea was the observation of markedly reduced resazurin

358   accumulation in the double mutant, where pump over-expression would be expected

359   to reduce accumulation of a wide range of substrates and confer the typical efflux-

360   based MDR phenotype observed.

361   To confirm the causative impact of these mutations, we used the same approach as

362   for the cefotaxime mutations where we re-introduced mutant and wild-type alleles of

363   *acrB* and *ramR* into mutants lacking these genes to observe the impact (Figure 5f).

364   AcrB R717L introduction to the *ΔacrB* background led to increased resistance only

365   against azithromycin, complementing perfectly the phenotype of the adapted and

366   evolved strain carrying the AcrB R717L mutation. RamR T18P introduction to the

367   *ΔramR* background led to an additional increase in MICs of azithromycin,

368   chloramphenicol, nalidixic acid and tetracycline, confirming the hypothesis that

369   overexpression of the efflux pump leads to an MDR response. These results confirm

370   that these are the mutations responsible for the resistant phenotypes observed after

371   exposure to azithromycin.

372   To investigate the impact of the R717L substitution on the structure and function of

373   AcrB, we performed molecular docking of azithromycin and erythromycin

374   (supplementary Figure S2, a-b) in the proximal binding site. The proximal binding

16

375   pocket is split into two distinct, yet overlapping macrolide binding sites, A and B. Site

376   A is known to be responsible for rifampicin binding, whereas, site B has been

377   associated with erythromycin binding and is located deeper into the proximal pocket

378   (30).

379   We first docked azithromycin in site B of the proximal binding pocket, producing a

380   model structure, which closely matches the experimental structure of AcrB with

381   erythromycin (3AOC.pbd, chain C, supplementary figure S2, a-b)(30). Our analysis

382   indicated that R717 is located too far away to directly interact with the drug, making it

383   unlikely for the observed coordination in site B to contribute to the observed

384   phenotype. To investigate whether R717 participates in earlier stages of the

385   substrate recognition pathway, we performed docking of azithromycin to site A,

386   located in the front part of the proximal binding pocket (Figure 4g). This showed

387   plausible coordination with direct involvement of R717, and also indicated a clear

388   energetic advantage of the R717 WT over R717L. In fact, R717L led to a radically

389   different coordination of azithromycin (Figure 4h, supplementary table S1),

390   rationalising the observed MDR phenotype.

391   **Drug resistance in biofilms is stable once selected but costs to virulence and**

392   **biofilm formation can be ameliorated by stress free passage**

393   We showed that control biofilms that have not been exposed to drugs rapidly

394   adapted to form better biofilms during the experiment (Figure 1f). However, when

395   these strains were tested for drug susceptibility, no changes were observed over

396   time (Figure 6a). There was also no correlation between biofilm ability and

397   antimicrobial susceptibility in these populations which were not exposed to any drugs

398   (Figure 6b). This shows that making more biomass does not alone affect antibiotic

399   susceptibility.

17

400   While we initially investigated whether biofilms have inherently altered susceptibility

401   to antibiotics using conventional susceptibility testing, we also tested whether

402   biofilms were more tolerant of drugs in context. To test whether biofilm-adapted

403   strains have a viability advantage when treated with antibiotics, we grew biofilms on

404   beads for 72 hours at 30°C, and then washed them and exposed them to a range of

405   ciprofloxacin concentrations (Figure 6c). To determine the survival rate, we isolated

406   and counted surviving cells. Survival was normalised against biofilms formed from

407   each strain unexposed to drug. We tested: a planktonic isolate which had been

408   exposed to ciprofloxacin (Cip-plank-L-S1), a control biofilm-adapted isolate not

409   exposed to any drug (biofilm-control-L-S1) and an exposed, biofilm adapted isolate

410   from the ciprofloxacin evolution experiment (Cip-biofilm-L-B-S3). The control biofilms

411   made significantly more biomass than the drug exposed biofilms but demonstrated

412   only a mild increase in survival to the drug treatment compared to the WT strain.

413   Biofilms formed by the drug-exposed planktonic lineage (adapted and highly

414   resistant to ciprofloxacin but with equivalent biofilm formation ability to the parent)

415   had also a mild increase in survival compared to WT biofilms. Interestingly, only

416   bacteria from the biofilm lineage exposed to ciprofloxacin exhibited a significant

417   survival increase even though this strain was no more resistant (by MIC) than the

418   planktonic mutant and made significantly less biofilm than the drug free control. This

419   suggests that neither specific resistance to ciprofloxacin or the ability to make more

420   biomass are enough to improve survival within a biofilm alone. To confirm these

421   results, we grew biofilms on coverslips for 72 hours at 30°C, treated them with 3

422   μg/mL ciprofloxacin for 90 minutes and carried out live/dead staining to visually

423   characterise survival by fluorescence microscopy (Figure 6d). Our first observation

424   was that, as expected, the different strains formed biofilms of variable density.

18

425   Survival was only obvious in the denser biofilm regions, where cells produced more

426   biomass and significant numbers of surviving cells were only observed in the

427   ciprofloxacin-exposed biofilm lineage. Visualisation of this biofilm showed denser

428   clusters of cells than the WT or biofilm-adapted lineage biofilms. Whilst the overall

429   level of biomass was not as high as drug free adapted controls for this strain, the

430   results suggest that a combination of improved biofilm formation and stress

431   adaptation are essential for biofilm viability and survival.

432   To test whether drug adaptation influences pathogenicity, we selected isolates from

433   different exposures and tested their virulence in the *Galleria mellonella* infection

434   model (Figure 6e, bar chart). Larvae were injected with strains representing different

435   biofilm and resistance phenotypes. Un-injected larvae as well as PBS controls were

436   included as appropriate and the wild type strain (14028S) was used as a reference.

437   In parallel we measured biofilm formation for all cultures used to inoculate larvae

438   using both the CV (Figure 6e, overlaid line graph on the right axis) and the CR

439   assay. We observed that strains with increased biofilm ability were the least

440   infectious, whereas isolates with weaker biofilm phenotypes were most pathogenic.

441   For example, biofilm-control-L-S1, which is a drug free control, biofilm-adapted

442   strain, caused the least deaths with a 95% survival rate. In comparison, Cip-biofilm-

443   M-B-S2, which is a drug-resistant but low-biofilm-forming strain, killed 50% of the

444   larvae. Hence, adaptation to the drug exposure had no obvious advantage for

445   pathogenicity. Our data suggests a strong correlation between pathogenicity and

446   biofilm formation but no association with resistance.

447   To test the stability of the phenotypes obtained during the course of the evolution

448   experiments, we selected resistant strains to the previous antibiotic exposures with

449   low and high biofilm forming abilities (see materials and methods) and put them

19

450   through a 24-hour passage, accelerated biofilm evolution experiment (Figure 6, f-i).

451   This was run for 10 days with passages every 24 hours without any antibiotics

452   present, to test whether the resistance and biofilm patterns change over time without

453   any selection. From each population, we isolated single strains and phenotyped

454   them for their biofilm ability and their susceptibility against the same panel of

455   antibiotics we used previously (see materials and methods). We observed that

456   resistance remained stable for most antibiotics (Figure 6f), while the overall ability of

457   the tested strains to form biofilms improved significantly over time (p<0.04, Figure

458   6g). We also looked individually at the strains with initially low biofilm ability and

459   decreased susceptibility (azi-biofilm-M-B-S2, cef-biofilm-L-A-S1) and we observed

460   that stability of resistance is highly dependent on the nature of the stress. The MIC of

461   azithromycin did not significantly change over time for the azithromycin resistant

462   strain (Figure 6h, orange line), whereas the initially cefotaxime resistant strain

463   exhibited significantly reduced susceptibility by the end of the accelerated

464   experiment (Figure 6i, purple line). In both cases, the biofilm formation of the strains

465   was recovered (Figure 6, h-i).

466

20

467 **Discussion**

468 To develop new antimicrobial strategies, it is important that we understand the

469 genetic mechanisms responsible for bacterial resistance in relevant contexts.

470 Although the evolution of antimicrobial resistance is often studied, previous work has

471 largely focused on planktonic cells and not bacterial biofilms. While it is commonly

472 accepted that biofilms are inherently highly drug resistant, surprisingly little work

473 explores how biofilms evolve in response to antimicrobial stress. One recent report

474 showed that *Acinetobacter* biofilms do adapt to sub-lethal exposure to ciprofloxacin

475 and that mechanisms of resistance were distinct to those seen in planktonic controls

476 (34). Here we address this question using *Salmonella* biofilms as a model system

477 with multiple drugs.

478 The intrinsic resistance of biofilms to antimicrobials has been attributed to both

479 unique structural characteristics of biofilms but also the wide range of growth states

480 of cells present within biofilms, including dormant or persister cells (35–39). We

481 investigated whether these already resistant communities evolve and adapt further

482 when exposed to sub-inhibitory drug stress. We found that biofilms are highly

483 sensitive to sub-inhibitory exposure to antibiotics, which rapidly selected for changes

484 in the populations. Different stresses selected distinct patterns of adaptation, some

485 of which were unique to the biofilm communities. There was no common response to

486 all three drugs tested, which strongly suggests that there is not a common or generic

487 mechanism for antimicrobial resistance seen in biofilms but instead adaptation highly

488 depends on the nature of the stress.

489 When cells were exposed to azithromycin or cefotaxime, both planktonic and biofilm

490 populations became resistant not only to the selective drug but also to several

21

491   different antibiotics, indicating mechanisms conferring MDR. Strikingly, both

492   azithromycin and cefotaxime selected for highly-resistant populations, but also with a

493   marked attenuation of biofilm formation. Lineages exposed to ciprofloxacin were able

494   to improve biofilm formation over time although this was delayed compared to control

495   biofilms. The ciprofloxacin results are consistent with a recent observation from

496   *Acinetobacter* biofilms, where biofilm formation was not compromised after exposure

497   to the drug (34). It is clear from our results that selection of resistance within a biofilm

498   can have a major impact on important phenotypes that impact on bacterial fitness

499   and survival in the real world.

500   To determine the mechanisms underlying susceptibility, we sequenced more than

501   100 strains covering the different exposures and time points and demonstrating a

502   range of distinct susceptibility and biofilm phenotypes. Azithromycin exposure

503   selected for the same mutations (changes in AcrB and RamR) in independent

504   lineages, and these emerged in a step-wise manner over the course of the evolution

505   experiment. Similarly, exposure to cefotaxime selected for mutants with altered AcrB

506   and EnvZ, with the same substitution within EnvZ observed in independent lineages.

507   The primary aim of this work was to identify mechanisms rather than the detailed

508   evolutionary dynamics of selection, however the presence of identical substitutions in

509   multiple lineages is strong evidence for the importance of these changes.

510   Ciprofloxacin exposure selected for a wider variety of mutations with much more

511   variation in phenotypes indicating multiple paths of evolution and resistance. The

512   difference between the drugs is likely to reflect the mechanisms of action and

513   resistance; there are multiple known chromosomal mechanisms of ciprofloxacin

514   resistance (including target site changes, porin loss, efflux) whereas high-level

515   resistance to cefotaxime and azithromycin is often a result of acquisition of specific

22

516   enzymes. In this closed system, acquisition of DNA is not possible, so cells are

517   constrained to mutation of the core genome to generate resistant mutants. This

518   hypothesis was supported by analysis of the mechanisms of resistance.

519   After analysing the sequencing results, we were able to identify novel mechanisms of

520   resistance against cefotaxime and azithromycin respectively, which we then

521   confirmed experimentally.

522   We showed that strains exposed to cefotaxime demonstrated a two-step selection of

523   resistance with an initial four-fold rise in cefotaxime MIC, followed by an eight-fold

524   increase. This was linked to an initial R397H substitution in the EnvZ protein followed

525   by an additional Q176K genetic substitution in AcrB. We showed that the EnvZ

526   R397H substitution alters the balance of porin production with down-regulation of the

527   major outer membrane pore, OmpF and up-regulation of the narrow outer membrane

528   pore, OmpC. EnvZ controls activity of OmpR, which is known to control the balance

529   of porin production as well as biofilm formation under low medium osmolarity

530   conditions (17,40). OmpF is well characterised as an entry point for β-lactams due to

531   the molecules' physiochemical properties, which makes entry possible through this

532   porin which has a larger pore size than OmpC (41,42). We showed that with OmpF

533   expression repressed, the cells are less permeable, leading to reduced levels of the

534   antibiotic in the cell and as a result decreased susceptibility. Whilst the EnvZ

535   substitution was selected in both planktonic and biofilm cultures only planktonic

536   cultures acquired the additional Q176K AcrB substitution, leading to even further

537   reduced drug accumulation and as a result, decreased susceptibility. To date, the

538   exact binding pocket responsible for recognition of cephalosporins, and β-lactams in

539   general, remains debatable with evidence pointing either to the proximal or the distal

540   binding pocket (25,43,44). Here, we showed that Q176K substitution is located in a

23

541   critically important position within the distal binding pocket of the protein, altering

542   significantly the binding dynamics of the pocket towards cephalosporins. We

543   hypothesise that this may lead to altered residence time in the pocket and result in

544   the observed macroscopic MDR effect. Significantly, our results are consistent with

545   prior data showing that Q176 is involved in substrate transport and coordination of

546   the chromogenic cephalosporin antibiotic nitrocefin in both docking and MD

547   simulation (25,29,45). Intriguingly, the orientation of cefotaxime in the binding pocket

548   was found to differ significantly from that of nitrocefin and cephalothin suggesting

549   multiple modes of β-lactam binding may exist within the distal binding pocket of AcrB

550   (Supplementary Figure S1, a-b, d).

551   Populations exposed to azithromycin also demonstrated a two-step selection, quickly

552   developing resistance to the drug with an 8-fold followed by a 16-fold increase in

553   azithromycin MIC. These changes were linked to two distinct amino acid

554   substitutions; AcrB R717L and RamR T18P. The AcrB substitution is located in the

555   proximal binding pocket, which is part of the principal drug entry and coordination

556   pathway for high molecular mass drugs and is predicted to impact substrate entry to

557   the pump. A role for R717 in the substrate pathway has previously been proposed

558   (29) and also shown to participate in the coordination of the related antibiotic,

559   rifampicin in at least one experimental structure (30). Docking of azithromycin into

560   the macrolide site A and B of the experimental structures, revealed that the R717 is

561   located far from the canonical site B, which is associated with erythromycin binding.

562   Therefore, this residue is more likely to participate in the earlier stages of the

563   substrate pathway in site A of the proximal pocket. Consistent with this interpretation,

564   we observed that the top docking pose of the azithromycin site A of the proximal

565   pocket brings it in direct contact with the R717 and as a result affected by the R717

24

566   substitution. This makes the pump more effective at exporting azithromycin out of the

567   cells and as a result, the population more resistant. The second substitution in RamR

568   resulted in the upregulation of this already "upgraded" AcrAB pump, leading to a 16x

569   rise in azithromycin MIC.

570   A small number of substitutions within AcrB have been identified and predicted to

571   change affinity for different drugs in the past (46). The substitutions identified in this

572   study have not been previously characterised for their role in resistance, which we

573   did here for the first time, providing strong genetic, phenotypic and structural

574   evidence for their functional impacts.

575   Both the mechanisms of resistance identified against azithromycin and cefotaxime

576   directly affect both membrane permeability and efflux activity of the cells. The nature

577   of these substitutions leads to cross-resistant phenotypes as accumulation of many

578   drugs is compromised by alterations of general porins and AcrAB. This is of critical

579   importance as exposure to a single drug can select for multi-drug resistant

580   populations with health-threatening implications.

581   We did however identify clear trade-offs between drug resistance and biofilm

582   formation. Although previous studies have associated exposure to sub-inhibitory

583   concentrations of azithromycin and cefotaxime with inhibition of biofilm formation

584   (47,48), the mechanisms identified in this study have not, to the best of our

585   knowledge, been associated with these antibiotics before. Although we showed that

586   biofilms respond and adapt to antibiotic stresses, we observed that this adaptation is

587   driven by the need to survive exposure to the drug and was not linked to biomass

588   production. Control biofilms passaged without stress made much larger biofilms over

589   time, but these improved biofilm forming lineages did not become more drug

25

590   resistant. To explore this surprising observation further, we grew biofilms of selected

591   strains representing a variety of biofilm formation and resistance phenotypes and

592   tested their ability to survive exposure to increasing ciprofloxacin concentrations. We

593   observed that only biofilms which had been exposed to ciprofloxacin were

594   significantly harder to kill. This reflects their possession of both a robust community

595   structure and drug-specific resistance mutations that makes them fitter in the specific

596   environment. Neither strains with increased resistance to ciprofloxacin but normal

597   biofilm capacity, nor those with normal drug sensitivity but increased biofilm capacity,

598   demonstrated a significant benefit when treated with ciprofloxacin. Based on these

599   results, we hypothesise that producing more biomass is not necessarily the best

600   solution to survive antibiotic exposure. Highly resistant biofilms may be more likely to

601   result from a combination of both structural and drug specific mechanisms.

602   Interestingly we did not identify mutations in pathways previously proposed to

603   contribute to persister cell formation, suggesting that these were not important in

604   adaption to the drug exposures in our experimental setup.

605   Biofilms play a crucial role in chronic infections and our observations suggested an

606   obvious fitness advantage of adapted biofilms over unexposed biofilm populations in

607   terms of drug resistance. To see if this impacts virulence we investigated the

608   pathogenicity of strains with different resistance and biofilm profiles, using the

609   *Galleria mellonella* infection model. We observed that mutations that rendered the

610   bacteria resistant to drugs had no significant impact on pathogenicity. However, the

611   biofilm ability of the strains was negatively correlated with pathogenicity, with strains

612   forming least biofilm being most virulent resulting in the lowest survival rates.

26

613   Having characterised a number of biofilm-related resistant phenotypes, we estimated

614   their stability in the absence of drug selective pressure using an accelerated biofilm

615   evolution experiment. Strains that had been exposed to ciprofloxacin and

616   azithromycin maintained their resistance profiles over extended passaging but

617   formed better biofilms. In contrast, cefotaxime exposed populations lost their

618   acquired resistance after a few passages whilst they became better biofilm formers.

619   This indicates that although stability of resistance is highly influenced by the nature

620   of the antimicrobial stress, bacteria can quickly adapt to a more sessile, community-

621   orientated lifestyle in the absence of drug. Analysis of azithromycin-exposed

622   populations which had improved their biofilm ability identified loss-of-function

623   mutations in cyclic di-GMP phosphodiesterase, YjcC. This is unsurprising as cyclic

624   di-GMP is well known for its role in biofilm formation in several organisms including

625   *Salmonella*, which harbours 12 proteins with GGDEF and 14 proteins with EAL

626   domains (49,50).

627   In conclusion we demonstrate here that biofilms are highly sensitive to stress from

628   low levels of antibiotics, rapidly adapt to drug pressure and that mechanisms of

629   resistance can incur costs to other important phenotypes. Using similar approaches

630   to those outlined here will help understand the impacts of drug exposure on biofilms

631   in many contexts. This can help inform how best to use antimicrobials and predict

632   how biofilms will respond to different stresses.

Materials and methods

Biofilm adaptation and evolution model

Salmonella enterica serovar Typhimurium 14028S was used as the parent strain to initiate all biofilm experiments in this study. This strain has been used as a model for *S.* Typhimurium biofilm studies by many groups including our own and has a fully closed and annotated reference genome (Accession number: CP001363). To study adaptation and evolution of *Salmonella* biofilms, we adapted a model described by the Cooper group (11). Bacteria were grown on 6 mm soda lime glass beads (Sigma, Z265950-1EA) for 72 hours in Lysogeny Broth (LB) with no salt. They were incubated in glass universal tubes containing 5 mL of the medium in horizontal position, with mild rocking at 40 rpm, at 30 ºC. For each passage, the beads were washed in PBS and transferred into fresh media with new sterile beads. The experiment was carried out at the presence of three clinically-important antibiotics; azithromycin, cefotaxime and ciprofloxacin at a final concentration of 10 μg/mL, 0.062 μg/mL and 0.015 μg/mL respectively. Eight independent lineages were included per exposure; four drug-exposed biofilm lineages, two drug-exposed planktonic cultures and two unexposed, bead-only control lineages. In each tube, three initially sterile beads were used, one to be transferred to the next lineage, one to be stored, and one from which cells were recovered for phenotyping. For storage, one bead per passage was frozen in 20 % glycerol. For phenotyping, the cells were isolated from the beads by vortexing in PBS for 30 seconds and then grown overnight in 1 mL of LB broth, before being stored in chronological order in deep-well plates in glycerol. The experiments were completed after 250 generations (17 passages) for the azithromycin and cefotaxime exposure and after 350 generations (24 passages) for the ciprofloxacin exposure. Populations from an early (first

658 passage), middle (half way point lineage) and late (final passage) time point were

659 chosen for study and from each, three single colonies were isolated, sub-cultured

660 and stored in 20% glycerol. These single-cell isolates, and their parent populations

661 were stored in deep-well 96-well plates and used for phenotyping by replicating the

662 bacteria onto appropriate media to test for fitness, biofilm ability, morphology and

663 susceptibility (replication used 'QRep 96 Pin Replicators', Molecular devices X5054).

664 Figure 1 shows an overview of the experimental setup and phenotyping procedure.

665 *Model optimisation*

666 To determine the optimum culture conditions for achieving the greatest cell carriage

667 of *S.* Typhimurium 14028S biofilms on the glass beads, biofilms were grown in 5 mL

668 LB without salt on 6 mm glass beads at four standard microbiological incubation

669 temperatures: 25 °C, 30 °C, 37 °C and 40 °C. The cell counts on beads grown at

670 each temperature was determined every 24 hours for 96 hours. Biofilms were

671 washed in 1 mL PBS and harvested via vortexing for 30 seconds. The harvested

672 cells were serially diluted in a microtiter tray containing 180 µL PBS and 5 µL was

673 spotted onto a square LB agar plate. The number of colony forming units was

674 calculated and the incubation conditions yielding the greatest amount of cells was

675 determined.

676 *Crystal violet assay (CV)*

677 To measure biofilm formation, selected strains were grown overnight in LB broth and

678 then diluted into 200 µL of LB-NaCl to give an OD of 0.01 in microtiter plates. The

679 plates were incubated at 30 °C for 48 hours, covered in gas-permeable seals before

680 wells were emptied and vigorously rinsed with water before staining. For staining,

681 200 µL of 0.1% CV was added to each well and incubated for 15 minutes at room

682 temperature. The crystal violet dye was then removed, and the wells were rinsed

683 with water. The dye bound to the cells was then dissolved in 70% ethanol and the

684 absorbance was measured at 590 nm in a plate reader (FLUOStar Omega, BMG

685 Labtech).

686 *Biofilm morphology*

687 To visually assess biofilms morphology, we replicated isolates stored in 96 deep-well

688 plates on 1% agar LB-NaCl plates, supplemented with 40 μg/mL Congo red (CR)

689 dye. The strains of interest were diluted to a final OD of 0.01 in a microtiter plate and

690 were then printed on the Congo red plates. The plates were incubated for 48 hours

691 at 30 °C before being photographed to capture colony morphology.

692 *Antimicrobial susceptibility testing*

693 To determine the minimum inhibition concentrations of antimicrobials against strains

694 of interest, we used the broth microdilution method (51) and the agar dilution method

695 (13), following the EUCAST guidelines. In both cases, Mueller-Hinton broth or agar

696 was used. Changes of less than two dilutions were not considered significant.

697 *Molecular Modelling and Antibiotic Docking*

698 For docking analysis, protein and ligand PDB files were first converted to PDBqt

699 format using Raccoon (52). AutoDock Vina (53) was used for unbiased flexible

700 docking simulations of ligands on protein structures using an optimal box size,

701 estimated according to the radius of giration of the ligands (grid-point spacing of 1

702 Å), centred on the predicted binding sites (supplementary table S1). The PyMOL

703 Molecular Graphics System, Version 2.0 Schrödinger, LLC. was used to visualize the

704 results. Formore information on model validation see supplementary materials.

705   *Extraction of DNA*

706   To extract genomic DNA for sequencing, selected strains were grown O/N in a 96-

707   deep-well plate in LB, at a final volume of 1.5 mL. Cells were recovered by

708   centrifugation at 3,500 g and were resuspended in 100 µL of lysis buffer (5 µg/mL

709   lysozyme, 0.1 mg/mL RNAse in Tris-EDTA, pH 8) per well. The resuspended cells

710   were then transferred in a new semi-skirted, low-bind PCR plate, secured with an

711   adhesive seal and incubated at 37 ºC, 1600 rpm for 25 minutes. 10 µL of a lysis

712   additive buffer (5% SDS, 1 mg/mL proteinase K, 1 mg/mL RNAse in Tris-EDTA, pH

713   8) was added in each well and the plate was sealed with PCR strip lids before being

714   incubated at 65 ºC, 1600 rpm for 25 minutes. The plate was briefly centrifuged and

715   100 µL were moved to a new PCR plate. For the DNA isolation, 50 µL of DNA-

716   binding magnetic beads (KAPA Pure beads, Roche diagnostics) were added in each

717   well and were incubated at room temperature for 5 minutes. The plate was then

718   placed on a magnetic base and the supernatant was removed by pipetting. The

719   beads were washed three times with 80% freshly-prepared ethanol. After removing

720   the last wash, the beads were left to dry for 2 minutes before eluting the DNA. For

721   the DNA elution, the plate was removed from the magnetic apparatus and 50 µL of

722   Tris-Cl were added to each well. The beads were pulled using the magnetic

723   apparatus and the isolated DNA was transferred to a new PCR plate. DNA

724   concentration was determined using the Qubit ds DNA HS Assay kit (Q32851)

725   following the manufacturer's instructions.

726   *Whole Genome sequencing*

727   Genomic DNA was normalised to 0.5 ng/µL with 10mM Tris-HCl. 0.9 µL of TD

728   Tagment DNA Buffer (Illumina Catalogue No. 15027866) was mixed with 0.09 µL

729   TDE1, Tagment DNA Enzyme (Illumina Catalogue No. 15027865) and 2.01 µL PCR

31

730   grade water in a master mix and 3ul added to a chilled 96 well plate. 2 μL of

731   normalised DNA (1ng total) was mixed with the 3 μL of the tagmentation mix and

732   heated to 55 ⁰C for 10 minutes in a PCR block. A PCR master mix was made up

733   using 4 ul kapa2G buffer, 0.4 μL dNTP's, 0.08 μL Polymerase and 4.52 μL PCR

734   grade water, contained in the Kap2G Robust PCR kit (Sigma Catalogue No.

735   KK5005) per sample and 11 μL added to each well need to be used in a 96-well

736   plate. 2 μL of each P7 and P5 of Nextera XT Index Kit v2 index primers (Illumina

737   Catalogue No. FC-131-2001 to 2004) were added to each well. Finally, the 5 μL

738   Tagmentation mix was added and mixed. The PCR was run with 72 ⁰C for 3 minutes,

739   95 ⁰C for 1 minute, 14 cycles of 95 ⁰C for 10 seconds, 55 ⁰C for 20 seconds and 72

740   ⁰C for 3 minutes. Following the PCR reaction, the libraries were quantified using the

741   Quant-iT dsDNA Assay Kit, high sensitivity kit (Catalogue No. 10164582) and run on

742   a FLUOstar Optima plate reader. Libraries were pooled following quantification in

743   equal quantities. The final pool was double-spri size selected between 0.5 and 0.7X

744   bead volumes using KAPA Pure Beads (Roche Catalogue No. 07983298001). The

745   final pool was quantified on a Qubit 3.0 instrument and run on a High Sensitivity

746   D1000 ScreenTape (Agilent Catalogue No. 5067-5579) using the Agilent Tapestation

747   4200 to calculate the final library pool molarity. The pool was run at a final

748   concentration of 1.8 pM on an Illumina Nextseq500 instrument using a Mid Output

749   Flowcell (NSQ® 500 Mid Output KT v2(300 CYS) Illumina Catalogue FC-404-2003)

750   and 15 pM on a Illumina MiSeq instrument. Illumina recommended denaturation and

751   loading recommendations which included a 1% PhiX spike in (PhiX Control v3

752   Illumina Catalogue FC-110-3001). Whole genome sequencing data has been

753   deposited in the Sequence Read Archive under PRJNA529870.

754

755   *Bioinformatics*

756   Sequence reads from the sequencer were uploaded on to virtual machines provided

757   by the MRC CLIMB (Cloud Infrastructure for Microbial Bioinformatics) project using

758   BaseMount (54). Quality filtering of the sequence reads was performed using

759   Trimmomatic (version 3.5) with default parameters (55). Trimmomatic's Illuminaclip

760   function was used to remove the Illumina adapters. The trimmed reads were then

761   assembled into contigs using SPAdes version 3.11.1 using default parameters (56).

762   To determine single nucleotide polymorphisms (SNPs) between the de novo

763   assembled Salmonella genomes and the parent genome. Snippy version 3.1 was

764   used using parameters recommended in (https://github.com/tseemann/snippy). The

765   Snippy-core from the Snippy tool box was used to determine the core SNPs. The full

766   genome alignment output by Snippy-core was used in subsequent phylogenetic

767   analyses, after removal of the published reference sequence (accession number

768   CP001363). All 4870267 sites were included in the analysis to avoid ascertainment

769   bias (57). A whole-genome phylogenetic tree was then inferred from the 63

770   sequences under the model HKY+G implemented in iq-tree (58). For the individual

771   population analyses the control sequences were removed, the trees were estimated

772   with iq-tree, using the HKY+G evolutionary model. All trees were arbitrarily rooted at

773   the cultivated parental sequence 14028S for visualisation purposes, and were

774   plotted with ggtree for R (59). Branch lengths are given in units of substitutions/site.

775   *Preparation of RNA samples for q-RT PCR*

776   RNA from biofilms was isolated using the SV Total RNA Isolation System kit

777   (Promega). RNA was extracted from the WT (14028S), cef-biofilm-M-D-S1

778   (EnvZR397H), cef-plank-L-S2 (EnvZR397H/ AcrB Q176K), azi-biofilm-E-B-S2 (AcrB

779   R717L) and azi-biofilm-M-B-S1(AcrB R717L/ RamR T18P) strains. These were

780   grown O/N at 37 °C in LB and then spotted on LB-NaCl agar plates and were grown

781   for 48 hours at 30 °C. Cells from each spot were then resuspended in 100 µL TE

782   containing 50 mg/mL lysozyme and were homogenised by vortexing. 75 µL RNA

783   Lysis Buffer (Promega kit), followed by 350 µL RNA Dilution Buffer (Promega kit)

784   were added to the cell suspensions, which were then mixed by inversion. Samples

785   were incubated at 70 °C for 3 minutes and centrifuged at 13,000 g for 10 minutes.

786   The supernatant was mixed with 200 µL 95 % ethanol and was then loaded on to the

787   spin columns provided by the kit. The columns were washed with 600 µL RNA Wash

788   Solution. DNAse mix was prepared following the Promega kit protocol and 50 µL

789   were directly added on the column membrane. After a 30 minutes incubation, 200 µL

790   DNAse Stop Solution was added and samples were centrifuged for 30 seconds.

791   Columns were washed with 600 µL RNA Wash Solution followed by 250 µL RNA

792   Wash Solution, and then centrifuged again for 1 minute to dry. RNA was eluted using

793   100 µL of nuclease-free water. RNA quantification was performed using the Qubit

794   RNA High Sensitivity Assay kit (Q32852).

795   *Quantitative Real-Time PCR (q-RT PCR)*

796   To determine expression levels of *ompC/F*, *csgA/B* and *ramA,* we performed q-RT

797   PCR using the Luna Universal One-Step RT-qPCR Kit from NEB (E3005), using the

798   Applied Biosystems^{TM} 7500 Real-Time PCR system. The primers used for the q-RT

799   PCR are listed in Table 2. Efficiency of the primers was calculated by generation of

800   calibration curves for each primer pair on serially diluted DNA samples. The R^2 of the

801   calibration curves calibrated was ≥0.98 for all the primer pairs used in this study.

802   RNA at a final amount of 50-100 ng was added to 10 µL final volume PCR reactions,

803   mixed with 400 nM of each primer. The cycle parameters were as follows: 10

34

804   minutes at 55 ºC (reverse transcription step), 1-minute denaturation at 95 ºC and 40

805   cycles of 10 seconds at 95 ºC and 1 minute at 60 ºC.

806   For each sample, two technical replicates from two biological replicates each were

807   included (four in total) per reaction. Controls with no reverse transcriptase were also

808   included for each RNA sample to eliminate DNA contamination.

809   To calculate expression levels, expression fold change was calculated using *gyrB*

810   expression as a reference. The relative expression was determined by calculating

811   the logarithmic base 2 of the difference between *gyrB* gene expression and target

812   gene expression per sample.

813   *Viability of cells within biofilms*

814   To determine the viability of cells within a biofilm, two approaches were used. The

815   first approach involved growing biofilms on glass beads for 72 hours. They were

816   washed in PBS to remove planktonic cells and were then challenged with different

817   concentrations of ciprofloxacin (0, 0.03, 0.3, 3 µg/mL) for 90 minutes. Beads were

818   washed again in PBS to remove any antibiotic and transferred into 1 mL of PBS

819   solution to an Eppendorf tube, where they were vigorously vortexed for 1 minute.

820   The cells recovered in PBS were serial diluted and spotted onto LB plates for CFU

821   counting the next day. For the second approach, we grew biofilms on glass slides for

822   72 hours. The slides were washed in PBS and were challenged with ciprofloxacin (3

823   µg/mL) for 90 minutes. They were washed in PBS and stained with a solution of 12

824   µM propidium iodide (PI) and 300 nM of SYTO 9 for 30 minutes. They were washed

825   in PBS and soaked in 70% ethanol to kill the cells before they were transferred to a

826   slide for microscopy. Fluorescence microscopy was performed in a Zeiss Axio

827   Imager M2.

35

828   *Galleria Infection model*

829   To test the pathogenicity of different mutants, we used the *Galleria mellonella* larvae

830   infection model. Wax worms were obtained from livefoods.co.uk. Similarly-sized

831   larvae with no signs of pupation or melanisation were chosen for injection. An initial

832   experiment was performed to calculate the infectious dose of *S.* Typhimurium

833   14028S in *G. mellonella*, which determined that an inoculation with approximately

834   20,000 CFU resulted in death of approximately half of 10 larvae after 72 hours. Once

835   this had been determined, overnight cultures of each strain were diluted in PBS to

836   replicate this inoculum concentration and 10 μL of this were injected into the second

837   hindmost left proleg of ten larvae. To check the concentration of each inoculum, 100

838   μL of each dilution were also plated onto LB agar and incubated overnight at 37°C.

839   CFUs were counted the next day and the inoculum concentration was confirmed.

840   Controls included in this experiment included larvae injected with PBS only and un-

841   injected larvae. All larvae were incubated at 37 °C and were checked three times a

842   day for 3 days to record the survival rate. The experiment was repeated on three

843   independent occasions, with 10 larvae randomly allocated per strain in each

844   experiment. Survival was calculated as the percentage of surviving larvae 48 hours

845   after injection (Figure 6, e).

846   *Cellular permeability assays*

847   To detect differences in cellular permeability to drugs between mutants, the

848   resazurin accumulation assay was used. The strains of interest were grown to

849   exponential phase, using a 1:100 inoculum from overnight cultures. The cells were

850   washed and resuspended in PBS normalising for cell density and they were mixed

851   with resazurin to a final volume of 100 μL (to give 10 μg/mL) in round-bottom

852   microtiter plates. Fluorescence was measured in the Omega FLUOstar plate reader

36

853   at excitation 544 nm and emission of 590 nm. Five replicates were included per

854   strain and resazurin-only reactions were used as controls. The assay was repeated

855   at least twice with reproducible results observed each time.

856   *Accelerated evolution experiments*

857   To test the phenotypic stability of strains recovered from the initial evolution

858   experiments, we performed an accelerated evolution experiment using six strains

859   representing a spectrum of biofilm forming capacities and drug resistance phenotypes

860   (WT, control-biofilm-L-S1, azi-biofilm-M-B-S2, azi-biofilm-M-B-S3, cef-biofilm-L-A-S1,

861   cip-biofilm-M-B-S2, cip-biofilm-L-B-S3). The strains were resuscitated from storage by

862   a 24-hour incubation at 37 °C in LB broth. After incubation, 50 μL of broth was added

863   to 5 mL of LB broth (without salt) containing three sterile glass beads and incubated

864   for 24 hours at 30 °C, until a biofilm was formed. Each bead was then washed in 1 mL

865   PBS to remove planktonic and loosely adherent cells. Two beads were stored in deep-

866   well plates containing 20 % glycerol for archiving and phenotyping. The third bead was

867   transferred to another tube of LB broth (without salt) containing three sterile glass

868   beads and passaged. This was repeated for ten passages, storing beads at each

869   timepoint.

870   Upon completion of ten passages, populations were recovered from passage five,

871   passage ten and the parental population for each mutant. From each population,

872   single colonies were picked after streaking out each population on LB agar and

873   incubating for 24 hours at 37 °C. Three colonies from each population were then

874   subcultured in LB broth. A population and three isolates from the start, middle and end

875   of the passage series were isolated and phenotyped for each mutant. Biofilm formation

876   was evaluated using the Congo Red and Crystal Violet assays. The agar dilution

37

877   methodology was used to assess the minimum inhibitory concentrations of antibiotics.

878   The average of the fold MIC change per antibiotic for all strains was calculated and

879   plotted against time. The average of biofilm formation, as determined by the crystal

880   violet assay, was calculated for all the strains per timepoint.

881   *Statistical analysis*

882   Biofilm forming ability was compared between strains or time points using linear mixed

883   models, with a random intercept of lineage where more than one lineage was included

884   for each strain or condition (Figures 1f and 6g).

885   Surviving cell counts were compared between strains using a linear mixed model with

886   a Poisson response, with random intercept of replicate, fixed effects of exposure, the

887   interaction between strain and exposure, and offset by the log of the average number

888   of cells counted in the 'unexposed' condition for each strain. Modelled means in each

889   exposure were then normalised by the average number of cells across all unexposed

890   conditions for plotting, such that the values shown represent the estimated proportion

891   of cells that would survive each exposure for each strain (Figure 6c). All error bars

892   reflect estimates +- one standard error.

893   *Strains and genetic manipulations*

894   *Escherichia coli* DH10b was used as a host for all cloning procedures.

895   Transformations of *E. coli* were carried out by heat shock of chemically competent *E.*

896   *coli* cells. Transformation of *Salmonella* was carried out by electroporation.

897   *Salmonella* electrocompetent cells were prepared as follows: *Salmonella* cells were

898   grown to early exponential phase (OD_{600nm} 0.2-0.3) in 50 mL of 2x YT, using a 1:100

899   inoculum from an overnight culture. The cells were centrifuged and washed once

900   with filter sterilised ice-cold water. They were left to incubate on ice for 1 hour before

901   they were pelleted at 3,000 g for 15 minutes. The cell pellet was resuspended in 1

902   mL of 10% filter-sterilised glycerol and 100 μL were used per transformation.

903   To create gene deletion mutants, we used the λ-red-based, gene doctoring

904   technique previously described in (60). For each deletion, two homologous regions

905   upstream and downstream of the genes of interest were amplified by PCR and were

906   cloned in MCS1 and MCS2 of the pDOC-K vector. The homologous regions were

907   300-400 bp in length and were designed to include the first and last 10 codons of the

908   gene to be deleted, to avoid any pleiotropic effects after deletion. For *acrB* and *ramR*

909   deletions, the upstream homologous regions were cloned EcoRI/ BamHI in MCS1

910   and the downstream ones as XhoI/ NheI in MCS2 of pDOC-K. For the *envZ* deletion,

911   the upstream homologous region was cloned EcoRI/ BamHI in MCS1 and the

912   downstream one as XhoI/ SpeI in MCS2.

913   For complementation of mutated genes, chromosomal integrations were created to

914   insert wild-type copies or mutated versions of genes of interest. This used a

915   modification of the gene doctoring system described above. pDOC-K was modified

916   to be used to deliver chromosomal gene integrations to the neutral intragenic region

917   downstream of *glms*. This chromosomal insertion site was proven to be neutral

918   through insertion of the reporter gene *lacZ*, where the mutant had no significant

919   difference in biofilm formation, efflux activity or competitive fitness (data not shown).

920   The integration vector (pDOC-K/ glms) was generated by cloning of the first

921   homologous region in MCS1 of pDOC-K, using EcoRI/ KpnI and the second

922   homologous region in MCS2 using XhoI/ NheI. The primer used for the amplification

923   of the second homologous region was designed to introduce a novel MCS (XhoI,

924   NdeI, SmaI, NotI, HindIII), upstream of the second homologous region which was

925 then used for the gene complementation constructs. Wild-type *ramR* and '*ramR-*

926 T18P' alleles were cloned XhoI/ HindIII in pDOC-K/ glms under the control of the

927 gene's native promoter. Wild-type *envZ* and '*envZ*-SNP' alleles were cloned XhoI/

928 HindIII in pDOC-K/ glms under the control of a constitutive plac promoter. For *acrB*

929 complementation, we used the pWKS30/ AcrB plasmid previously described in (61),

930 expression of the gene is under the control of the pBAD system and induction was

931 achieved with the use of 0.5% arabinose.

932 For induction of chromosomal integrations either for deletion or complementation of

933 a gene, the strain to be modified was transformed with the pDOC-K vector variant

934 and the pACBSCE helper plasmid carrying the λ-red genes. A single colony carrying

935 both plasmids was grown in 500 μL of LB, at 37 °C for 4 hours. The cells were

936 pelleted and washed three times in filter sterilized LB. They were then resuspended

937 in 500 μL of 0.1x LB supplemented with 0.3% arabinose and incubated at 37 °C for

938 2-3 hours for induction. 100 μL were plated on LB plates supplemented with 25 μg/

939 mL kanamycin and 5% sucrose. The plates were incubated overnight at 37 °C.

940 Single colonies were checked for chromosomal alterations using colony PCR with

941 primers annealing outside of the region to be modified. The plasmids were removed

942 by sub culturing the positive clones on kanamycin-supplemented plates and testing

943 them for chloramphenicol and ampicillin sensitivity until the plasmids were

944 completely removed.

945 For 'double deletions' and/or complementations, the kanamycin cassette, introduced

946 by the first chromosomal modification, was removed using the FLP sites flanking the

947 cassette. The strains were transformed by electroporation with the pCP20 vector,

948 carrying the genes for flippase activity, and recovered on LB agar plates

949 supplemented with 50 μg/mL ampicillin at 30 °C. The kanamycin cassette removal

950   was confirmed by colony PCR and the positive clones were sub-cultured on LB agar

951   at 37-42 ^{o}C. Removal of the plasmid was confirmed by testing the colonies'

952   sensitivity to ampicillin.

953

954   **Acknowledgements**

965   *Transparency declaration*

966   The funders had no role in study design, data collection and analysis, decision to publish, or

967   preparation of the manuscript

References

1. O'Neill J, The Review on Antimicrobial Resistance. Infection prevention, control and surveillance: Limiting the development and spread of drug resistance. London, UK; 2016 Mar.

2. Blair JMA, Webber MA, Baylay AJ, Ogbolu DO, Piddock LJV. Molecular mechanisms of antibiotic resistance. Nat Rev Microbiol. 2015 Jan;13(1):42–51.

3. Webber MA, Whitehead RN, Mount M, Loman NJ, Pallen MJ, Piddock LJV. Parallel evolutionary pathways to antibiotic resistance selected by biocide exposure. J Antimicrob Chemother. 2015 Aug;70(8):2241–2248.

4. Hughes D, Andersson DI. Selection of resistance at lethal and non-lethal antibiotic concentrations. Curr Opin Microbiol. 2012 Oct;15(5):555–560.

5. Marcusson LL, Frimodt-Møller N, Hughes D. Interplay in the selection of fluoroquinolone resistance and bacterial fitness. PLoS Pathog. 2009 Aug 7;5(8):e1000541.

6. Costerton JW, Cheng KJ, Geesey GG, Ladd TI, Nickel JC, Dasgupta M, et al. Bacterial biofilms in nature and disease. Annu Rev Microbiol. 1987;41:435–464.

7. Sauer K, Camper AK, Ehrlich GD, Costerton JW, Davies DG. Pseudomonas aeruginosa displays multiple phenotypes during development as a biofilm. J Bacteriol. 2002 Feb;184(4):1140–1154.

8. Miyaue S, Suzuki E, Komiyama Y, Kondo Y, Morikawa M, Maeda S. Bacterial Memory of Persisters: Bacterial Persister Cells Can Retain Their Phenotype for Days or Weeks After Withdrawal From Colony-Biofilm Culture. Front Microbiol. 2018 Jun 26;9:1396.

9. Cooper VS. Experimental Evolution as a High-Throughput Screen for Genetic Adaptations. mSphere. 2018 Jun;3(3).

10. Martin M, Hölscher T, Dragoš A, Cooper VS, Kovács ÁT. Laboratory evolution of microbial interactions in bacterial biofilms. J Bacteriol. 2016 Oct 1;198(19):2564–2571.

11. Poltak SR, Cooper VS. Ecological succession in long-term experimentally evolved biofilms produces synergistic communities. ISME J. 2011 Mar;5(3):369–378.

12. Whitehead RN, Overton TW, Kemp CL, Webber MA. Exposure of Salmonella enterica serovar Typhimurium to high level biocide challenge can select multidrug resistant mutants in a single step. PLoS One. 2011 Jul 29;6(7):e22833.

13. Determination of minimum inhibitory concentrations (MICs) of antibacterial agents by agar dilution. Clin Microbiol Infect. 2000 Sep;6(9):509–515.

14. Ostrer L, Khodursky RF, Johnson JR, Hiasa H, Khodursky A. Analysis of mutational patterns in quinolone resistance-determining regions of GyrA and ParC of clinical isolates. Int J Antimicrob Agents. 2018 Dec 21;

15. Wang Y, Huang WM, Taylor DE. Cloning and nucleotide sequence of the Campylobacter jejuni gyrA gene and characterization of quinolone resistance mutations. Antimicrob Agents Chemother. 1993 Mar;37(3):457–463.

16. Yoshida H, Bogaki M, Nakamura M, Nakamura S. Quinolone resistance-determining region in the DNA gyrase gyrA gene of Escherichia coli. Antimicrob Agents Chemother. 1990 Jun;34(6):1271–1272.

17. Cai SJ, Inouye M. EnvZ-OmpR interaction and osmoregulation in Escherichia coli. J Biol Chem. 2002 Jul 5;277(27):24155–24161.

18. Tipton KA, Rather PN. An ompR-envZ Two-Component System Ortholog Regulates Phase Variation, Osmotic Tolerance, Motility, and Virulence in Acinetobacter baumannii Strain AB5075. J Bacteriol. 2017 Feb 1;199(3).

19. Jubelin G, Vianney A, Beloin C, Ghigo J-M, Lazzaroni J-C, Lejeune P, et al. CpxR/OmpR interplay regulates curli gene expression in response to osmolarity in Escherichia coli. J Bacteriol. 2005 Mar;187(6):2038–2049.

20. Martínez-Martínez L, Conejo MC, Pascual A, Hernández-Allés S, Ballesta S, Ramírez De Arellano-Ramos E, et al. Activities of imipenem and cephalosporins against clonally related strains of Escherichia coli hyperproducing chromosomal beta-lactamase and showing altered porin profiles. Antimicrob Agents Chemother. 2000 Sep;44(9):2534–2536.

21. Lovelle M, Mach T, Mahendran KR, Weingart H, Winterhalter M, Gameiro P. Interaction of cephalosporins with outer membrane channels of Escherichia coli. Revealing binding by fluorescence quenching and ion conductance fluctuations. Phys Chem Chem Phys. 2011 Jan 28;13(4):1521–1530.

22. Nikaido H. Crossing the envelope: how cephalosporins reach their targets. Clin Microbiol Infect. 2000;6 Suppl 3:22–26.

23. Prigent-Combaret C, Brombacher E, Vidal O, Ambert A, Lejeune P, Landini P, et al. Complex regulatory network controls initial adhesion and biofilm formation in Escherichia coli via regulation of the csgD gene. J Bacteriol. 2001 Dec;183(24):7213–7223.

24. Pos KM. Drug transport mechanism of the AcrB efflux pump. Biochim Biophys Acta. 2009 May;1794(5):782–793.

25. Vargiu AV, Nikaido H. Multidrug binding properties of the AcrB efflux pump characterized by molecular dynamics simulations. Proc Natl Acad Sci USA. 2012 Dec 11;109(50):20637–20642.

26. Nikaido H, Pagès J-M. Broad-specificity efflux pumps and their role in multidrug resistance of Gram-negative bacteria. FEMS Microbiol Rev. 2012 Mar;36(2):340–363.

27. Murakami S, Nakashima R, Yamashita E, Matsumoto T, Yamaguchi A. Crystal structures of a multidrug transporter reveal a functionally rotating mechanism. Nature. 2006 Sep 14;443(7108):173–179.

28. Sjölund-Karlsson M, Joyce K, Blickenstaff K, Ball T, Haro J, Medalla FM, et al. Antimicrobial susceptibility to azithromycin among Salmonella enterica isolates from the United States. Antimicrob Agents Chemother. 2011 Sep;55(9):3985–3989.

29. Husain F, Nikaido H. Substrate path in the AcrB multidrug efflux pump of Escherichia coli. Mol Microbiol. 2010 Oct;78(2):320–330.

30. Nakashima R, Sakurai K, Yamasaki S, Nishino K, Yamaguchi A. Structures of the multidrug exporter AcrB reveal a proximal multisite drug-binding pocket. Nature. 2011 Nov 27;480(7378):565–569.

31. Yamasaki S, Nikaido E, Nakashima R, Sakurai K, Fujiwara D, Fujii I, et al. The crystal structure of multidrug-resistance regulator RamR with multiple drugs. Nat Commun. 2013;4:2078.

32. Abouzeed YM, Baucheron S, Cloeckaert A. ramR mutations involved in efflux-mediated multidrug resistance in Salmonella enterica serovar Typhimurium. Antimicrob Agents Chemother. 2008 Jul;52(7):2428–2434.

33. Eicher T, Cha H, Seeger MA, Brandstätter L, El-Delik J, Bohnert JA, et al. Transport of drugs by the multidrug transporter AcrB involves an access and a deep binding pocket that are separated by a switch-loop. Proc Natl Acad Sci USA. 2012 Apr 10;109(15):5687–5692.

34. Santos-Lopez A, Marshall CW, Scribner MR, Snyder D, Cooper VS. Biofilm-dependent evolutionary pathways to antibiotic resistance. BioRxiv. 2019 Mar 19;

35. Høiby N, Bjarnsholt T, Givskov M, Molin S, Ciofu O. Antibiotic resistance of bacterial biofilms. Int J Antimicrob Agents. 2010 Apr;35(4):322–332.

36. Stewart PS. Theoretical aspects of antibiotic diffusion into microbial biofilms. Antimicrob Agents Chemother. 1996 Nov;40(11):2517–2522.

37. Anderl JN, Franklin MJ, Stewart PS. Role of antibiotic penetration limitation in Klebsiella pneumoniae biofilm resistance to ampicillin and ciprofloxacin. Antimicrob Agents Chemother. 2000 Jul;44(7):1818–1824.

38. de la Fuente-Núñez C, Reffuveille F, Fernández L, Hancock REW. Bacterial biofilm development as a multicellular adaptation: antibiotic resistance and new therapeutic strategies. Curr Opin Microbiol. 2013 Oct;16(5):580–589.

39. Mah TF, O'Toole GA. Mechanisms of biofilm resistance to antimicrobial agents. Trends Microbiol. 2001 Jan;9(1):34–39.

40. Silva IN, Pessoa FD, Ramires MJ, Santos MR, Becker JD, Cooper VS, et al. The OmpR Regulator of Burkholderia multivorans Controls Mucoid-to-Nonmucoid Transition and Other Cell Envelope Properties Associated with Persistence in the Cystic Fibrosis Lung. J Bacteriol. 2018 Sep 1;200(17).

41. Benz R, Schmid A, Hancock RE. Ion selectivity of gram-negative bacterial porins. J Bacteriol. 1985 May;162(2):722–727.

42. Masi M, Réfregiers M, Pos KM, Pagès J-M. Mechanisms of envelope permeability and antibiotic influx and efflux in Gram-negative bacteria. Nat Microbiol. 2017 Feb 22;2:17001.

43. Kobayashi N, Tamura N, van Veen HW, Yamaguchi A, Murakami S. β-Lactam selectivity of multidrug transporters AcrB and AcrD resides in the proximal binding pocket. J Biol Chem. 2014 Apr 11;289(15):10680–10690.

44. Yu EW, Aires JR, McDermott G, Nikaido H. A periplasmic drug-binding site of the AcrB multidrug efflux pump: a crystallographic and site-directed mutagenesis study. J Bacteriol. 2005 Oct;187(19):6804–6815.

45. Takatsuka Y, Chen C, Nikaido H. Mechanism of recognition of compounds of diverse structures by the multidrug efflux pump AcrB of Escherichia coli. Proc Natl Acad Sci USA. 2010 Apr 13;107(15):6559–6565.

46. Blair JMA, Bavro VN, Ricci V, Modi N, Cacciotto P, Kleinekathöfer U, et al. AcrB drug-binding pocket substitution confers clinically relevant resistance and altered substrate specificity. Proc Natl Acad Sci USA. 2015 Mar 17;112(11):3511–3516.

47. Wang A, Wang Q, Kudinha T, Xiao S, Zhuo C. Effects of Fluoroquinolones and Azithromycin on Biofilm Formation of Stenotrophomonas maltophilia. Sci Rep. 2016 Jul 13;6(1):29701.

48. Baothong S, Sitthisak S, Kunthalert D. In vitro interference of cefotaxime at subinhibitory concentrations on biofilm formation by nontypeable Haemophilus influenzae. Asian Pac J Trop Biomed. 2016 Sep;6(9):745–750.

1110   49.   Simm R, Morr M, Kader A, Nimtz M, Römling U. GGDEF and EAL domains
1111   inversely regulate cyclic di-GMP levels and transition from sessility to motility.
1112   Mol Microbiol. 2004 Aug;53(4):1123–1134.

1113   50.   Ahmad I, Lamprokostopoulou A, Le Guyon S, Streck E, Barthel M, Peters V, et
1114   al. Complex c-di-GMP signaling networks mediate transition between virulence
1115   properties and biofilm formation in Salmonella enterica serovar Typhimurium.
1116   PLoS One. 2011 Dec 2;6(12):e28351.

1117   51.   EUCAST reading guide for broth microdilution.

1118   52.   Forli S, Huey R, Pique ME, Sanner MF, Goodsell DS, Olson AJ. Computational
1119   protein-ligand docking and virtual drug screening with the AutoDock suite. Nat
1120   Protoc. 2016 May;11(5):905–919.

1121   53.   Trott O, Olson AJ. AutoDock Vina: improving the speed and accuracy of
1122   docking with a new scoring function, efficient optimization, and multithreading. J
1123   Comput Chem. 2010 Jan 30;31(2):455–461.

1124   54.   Connor TR, Loman NJ, Thompson S, Smith A, Southgate J, Poplawski R, et al.
1125   CLIMB (the Cloud Infrastructure for Microbial Bioinformatics): an online
1126   resource for the medical microbiology community. Microb Genom. 2016 Sep
1127   20;2(9):e000086.

1128   55.   Bolger AM, Lohse M, Usadel B. Trimmomatic: a flexible trimmer for Illumina
1129   sequence data. Bioinformatics. 2014 Aug 1;30(15):2114–2120.

1130   56.   Nurk S, Bankevich A, Antipov D, Gurevich A, Korobeynikov A, Lapidus A, et al.
1131   Assembling Genomes and Mini-metagenomes from Highly Chimeric Reads. In:
1132   Deng M, Jiang R, Sun F, Zhang X, editors. Research in computational
1133   molecular biology. Berlin, Heidelberg: Springer Berlin Heidelberg; 2013. p. 158–
1134   170.

1135   57.   Tamuri A, Goldman N. Avoiding ascertainment bias in the maximum likelihood
1136   inference of phylogenies based on truncated data. BioRxiv. 2017 Sep 9;

1137   58.   Nguyen L-T, Schmidt HA, von Haeseler A, Minh BQ. IQ-TREE: a fast and
1138   effective stochastic algorithm for estimating maximum-likelihood phylogenies.
1139   Mol Biol Evol. 2015 Jan;32(1):268–274.

1140   59.   Yu G, Smith DK, Zhu H, Guan Y, Lam TT-Y. *ggtree*: an *R* package for
1141   visualization and annotation of phylogenetic trees with their covariates and
1142   other associated data. Methods Ecol Evol. 2016 Aug;

1143   60.   Lee DJ, Bingle LEH, Heurlier K, Pallen MJ, Penn CW, Busby SJW, et al. Gene
1144   doctoring: a method for recombineering in laboratory and pathogenic
1145   Escherichia coli strains. BMC Microbiol. 2009 Dec 9;9:252.

1146 61. Baugh S, Ekanayaka AS, Piddock LJV, Webber MA. Loss of or inhibition of all
1147   multidrug resistance efflux pumps of Salmonella enterica serovar Typhimurium
1148   results in impaired ability to form a biofilm. J Antimicrob Chemother. 2012
1149   Oct;67(10):2409–2417.

1150 62. Jarvik T, Smillie C, Groisman EA, Ochman H. Short-term signatures of
1151   evolutionary change in the Salmonella enterica serovar typhimurium 14028
1152   genome. J Bacteriol. 2010 Jan;192(2):560–567.

1153

1154 **Figures**
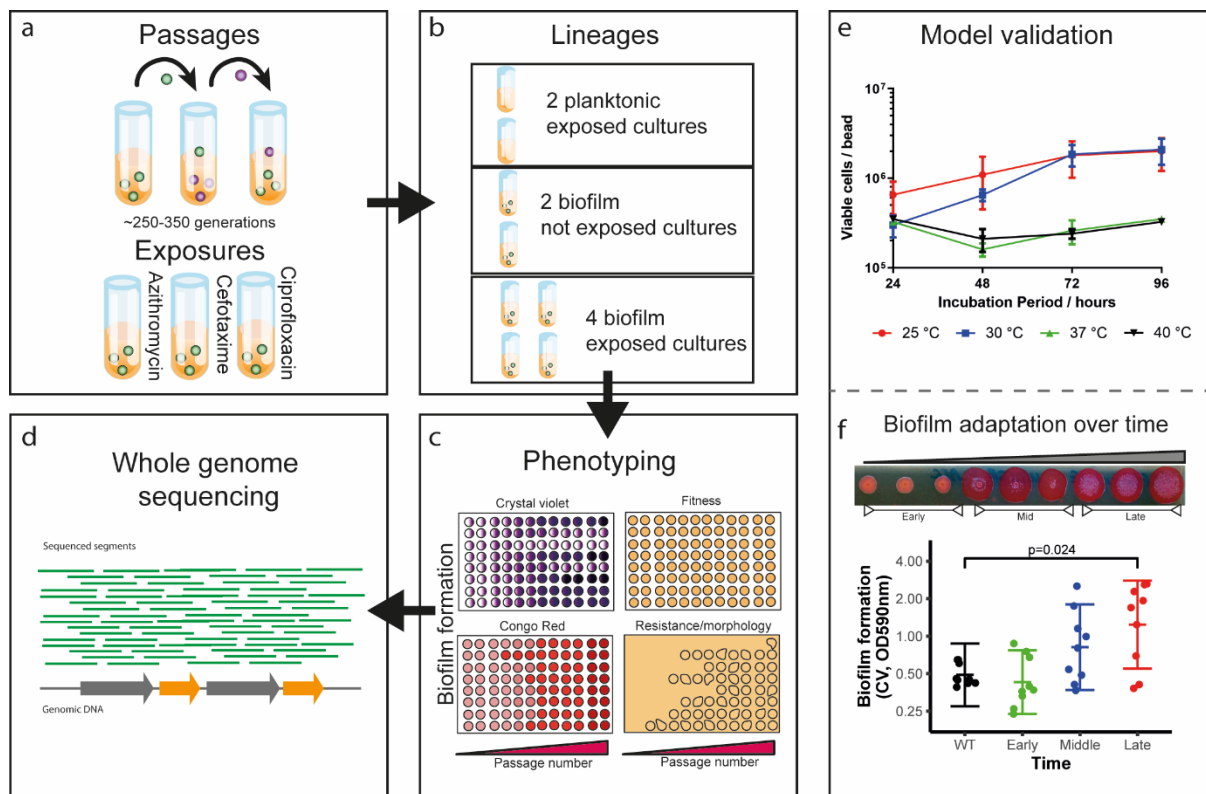
1155

Figure 1: Salmonella biofilm adaptation model. a, Sterile glass beads were used for the establishment of Salmonella biofilms. Three antibiotics were selected and used as stressors; azithromycin, cefotaxime and ciprofloxacin. b, For each experiment, eight independent lineages were ran in parallel; two planktonic controls, exposed to the drug, with no beads present; two bead controls, not exposed to the drug, and four independent lineages, exposed to the drug on beads. c, Passages and sampling were carried out every 72 hours at 30 °C and the cells isolated were stored and phenotyped for biofilm formation, fitness, susceptibility etc. d, Over 100 strains (populations and single-cell isolates) were selected and sequenced based on their phenotypic characteristics. e, To determine the right experimental conditions for the evolution experiment, cells were recovered and counted from biofilms grown for different periods of time, at different temperatures. This showed that the maximum cell carriage is achieved by 72 h at either 25 °C or 30 °C. Dots indicate average from 4 replicates and error bars show standard error f. To determine whether bacteria adapt to the bead model, biofilm formation was monitored over time by visualisation on Congo red-supplemented plates and by the Crystal Violet assay (OD:590nm), using the unexposed bead control lineages. The strains quickly adapted and produced significantly more biomass compared to the WT by the end of the experiment. Each dot represents single cell strains isolated from different timepoints. Error bars reflect estimated +/- one standard error.

1176
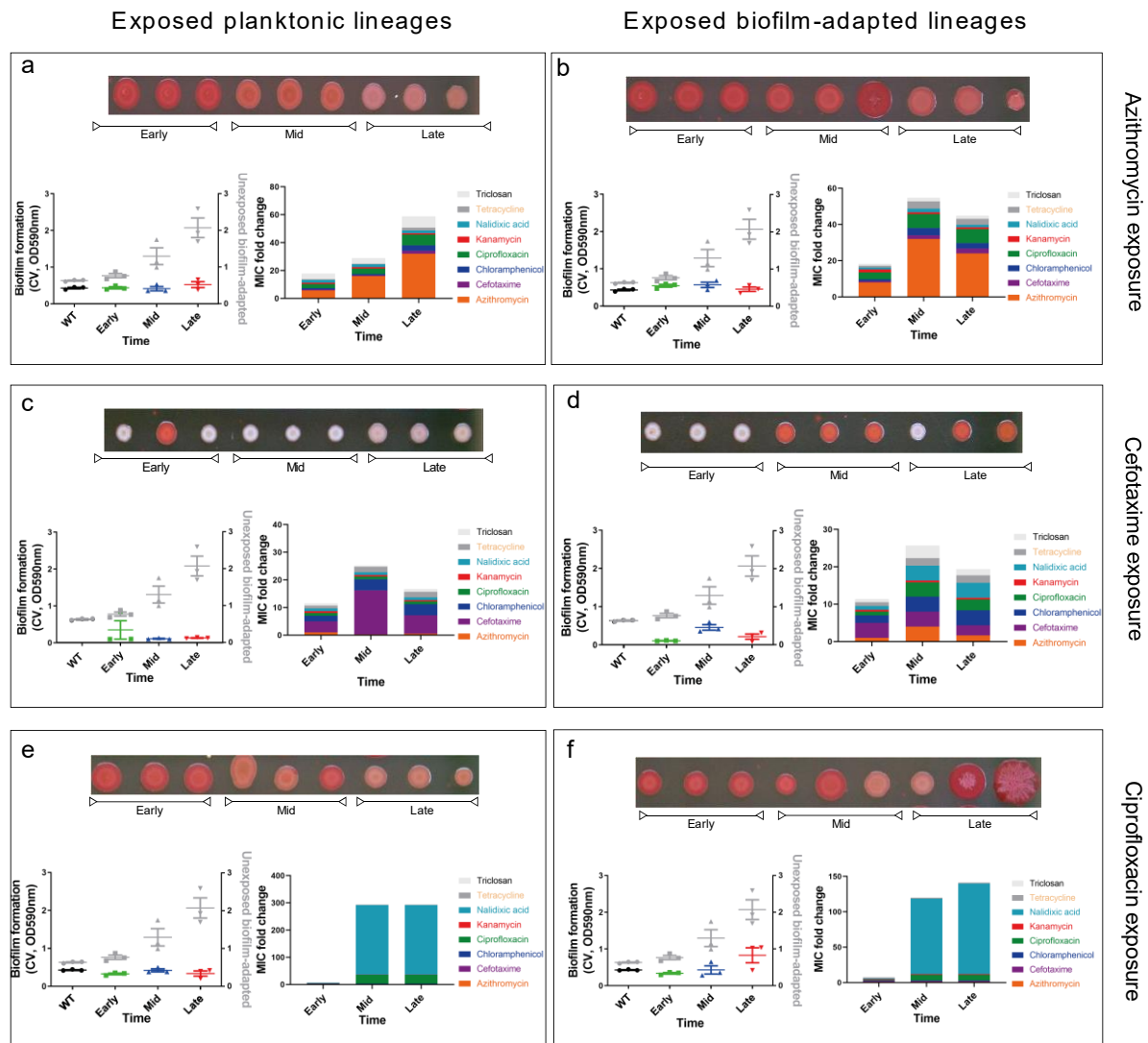1177
1178
1179
1180

Figure 2: Biofilms adapt to antibiotic stress, with diverse effects on biofilm formation. *Planktonic and biofilm populations, exposed to azithromycin (**a-b**), cefotaxime (**c-d**) and ciprofloxacin (**e-f**) were isolated at different timepoints during the evolution experiment (early, mid, late). Panels on the left show data from planktonic lineages, panels on the right from biofilm lineages. Three single isolates per timepoint were tested for their biofilm ability and susceptibility. Biofilm formation was measured by the Crystal Violet assay and on Congo Red plates. Unexposed biofilm lineages were used as a reference to biofilm adaptation (results shown in grey on CV graphs). Antibiotic susceptibility was determined by measuring the MIC values for a panel of different antimicrobials (azithromycin, cefotaxime, chloramphenicol, ciprofloxacin, kanamycin, nalidixic acid, tetracycline and triclosan). Stacked bars were generated by stacking the average MICs for each antibiotic (colour-coded), from three single cell isolates **a-b,** Both planktonic and biofilm isolates, exposed to azithromycin, developed resistance to azithromycin as well as decreased susceptibility to cefotaxime, chloramphenicol, ciprofloxacin, nalidixic acid, tetracycline and triclosan. Biofilm adaptation was inhibited in the biofilm lineages. **c-d,** Planktonic lineages, exposed to cefotaxime, rapidly developed resistance to cefotaxime. Biofilms under the same exposure exhibited an MDR response. Biofilm adaptation of both planktonic and biofilm lineages was completely compromised leading to pale colonies on CR plates. **e-f,** Planktonic and biofilm lineages exposed to ciprofloxacin adapted to the stress by*

1202 *developing resistance to the stressor. Biofilm adaptation was delayed compared to the*
1203 *unexposed control lineages but significantly increased by the end of the experiment.*
1204
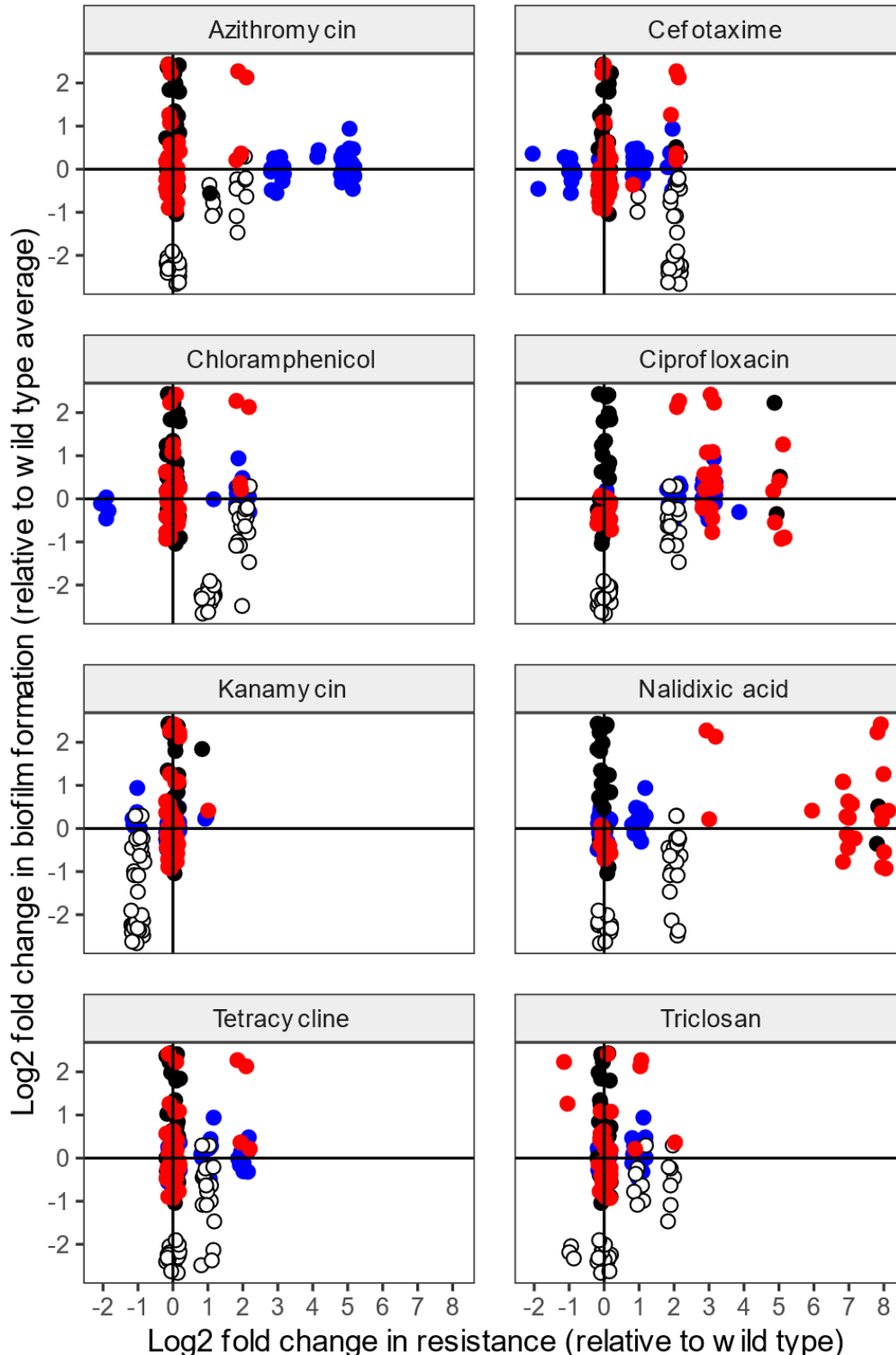
Figure 3: **Correlations between resistance and biofilm formation selected by different antibiotics. a-h,** *Fold change in MIC for each antibiotic was compared against the fold change in biofilm formation. Single isolates were characterised; with each dot on the graphs representing an individual isolate from each evolution experiment (blue: azithromycin, white: cefotaxime, red: ciprofloxacin, black: drug-free controls). The parent strain average, used as a reference, is represented as point '0,0'*

1211   *on the graphs. Azithromycin and cefotaxime exposed isolates became less*
1212   *susceptible not only to the stressor but also to other antimicrobials. Ciprofloxacin-*
1213   *exposed isolates only became resistant to fluoroquinolones. Biofilm formation was*
1214   *heavily compromised in cefotaxime-exposed strains. Azithromycin inhibited biofilm*
1215   *formation with some strains exhibiting slightly reduced levels of biofilm formation,*
1216   *whereas ciprofloxacin did not have a significant effect on biofilm adaptation.*
1217

1218

1219
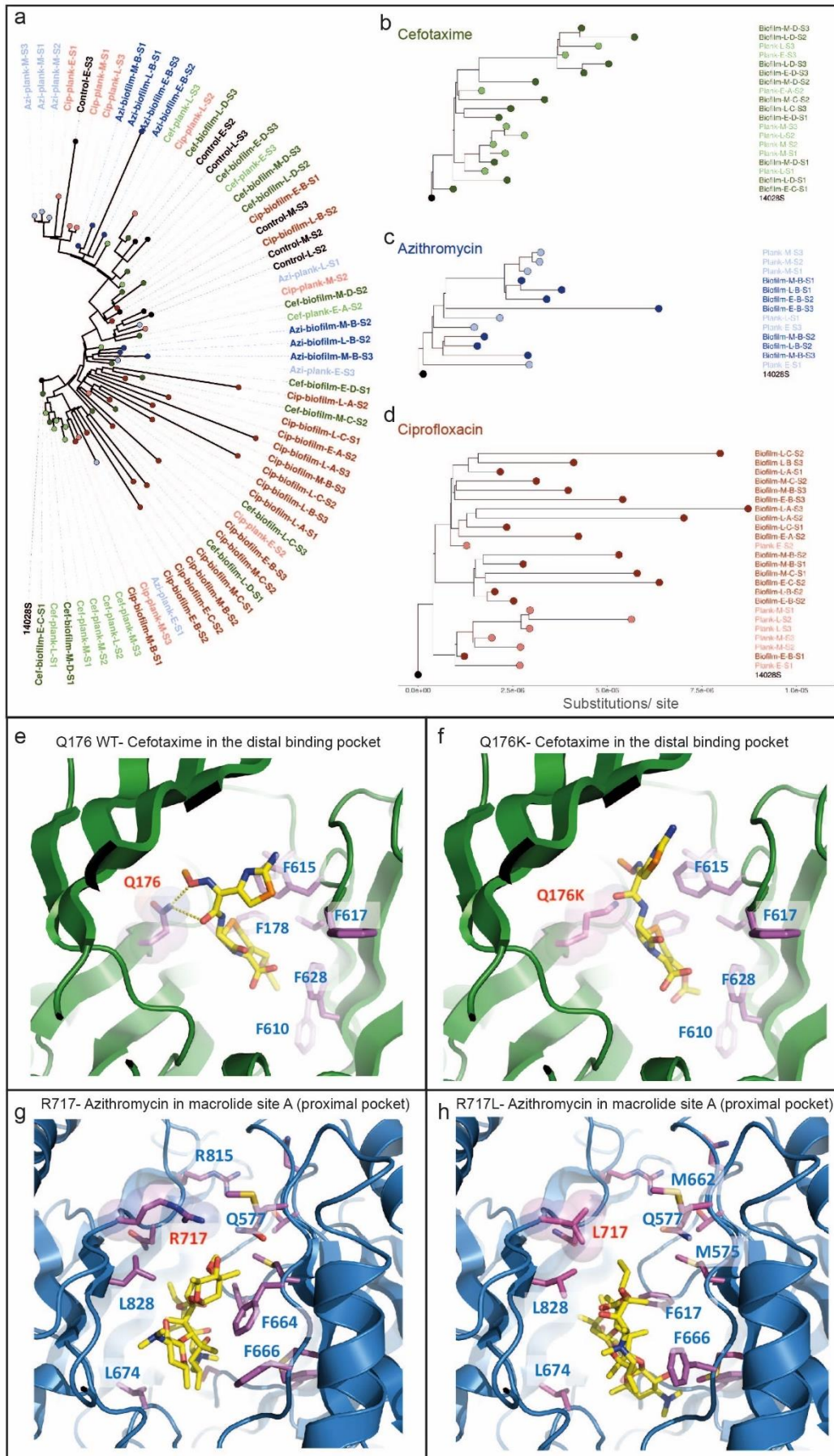
1220 **Figure 4. Phylogenetic analysis and AcrB modelling. a,** *Universal phylogenetic*
1221 *tree based on full genome alignment, showing diversity of strains exposed to*
1222 *azithromycin, cefotaxime and ciprofloxacin. Azithromycin and cefotaxime selected for*
1223 *mutants that followed a distinct evolution pattern, whereas ciprofloxacin-exposed*
1224 *strains evolved and responded to the stress in various ways. S. Typhimurium*
1225 *14028S (CP001363) was used as the reference strain and the tree was arbitrarily*
1226 *rooted at the cultivated parental sequence 14028S.* **b-d,** *Individual trees were*
1227 *generated for cefotaxime, azithromycin and ciprofloxacin-exposed strains. Dark dots*
1228 *indicate biofilm lineages, light dots planktonic lineages. Phylogenetic variations*
1229 *between biofilms and planktonic cultures were observed, indicating unique*
1230 *mechanisms of resistance between the two states.* **e,** *Cefotaxime binding to the*
1231 *distal binding pocket of AcrB (4DX5, chain B). Q176 is involved in the coordination of*
1232 *cephalosporin molecules in the binding pocket.* **f,** *Upon substitution with lysine*
1233 *(Q176K), the free energy of binding changed significantly, potentially resulting in*
1234 *reduced residence time of the drug in the pocket and hence, increased efflux* **g,**
1235 *Azithromycin docking to macrolide site A of the proximal binding pocket of AcrB*
1236 *(3AOB, chain C). R717 exhibits a direct involvement in macrolide coordination in the*
1237 *pocket.* **h,** *Substitution with leucine (R717L) led to radically altered coordination of*
1238 *azithromycin in the pocket.*

1239
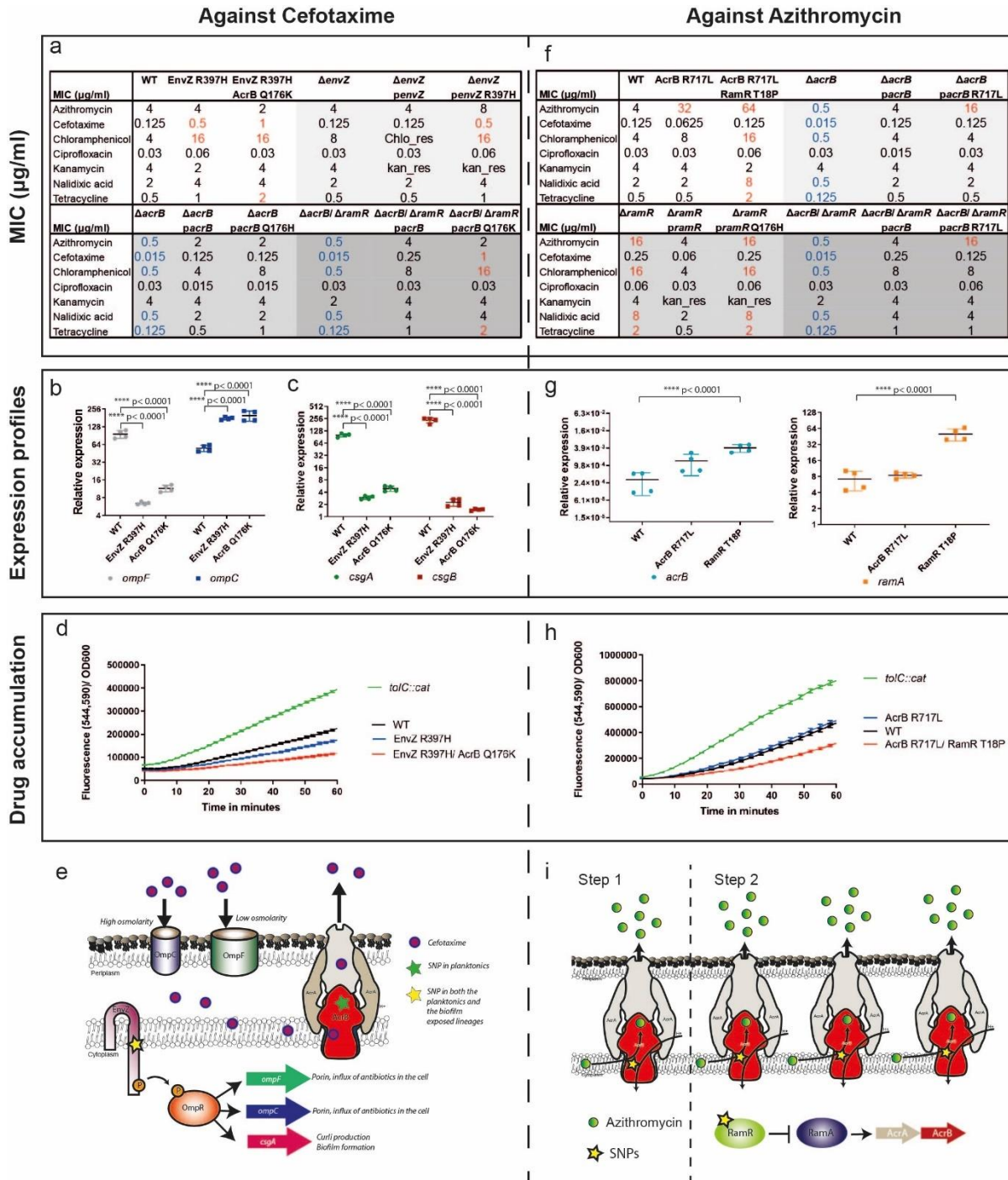
1240

Figure 5: Proposed novel mechanism of resistance to cefotaxime and azithromycin. a-i, *Cefotaxime and azithromycin exposed isolates exhibiting decreased susceptibility, were whole-genome-sequenced and genetic variations were identified.* **a,** *Cefotaxime exposed isolates from the middle timepoint carried the R397H substitution in EnvZ leading to reduced susceptibility to cefotaxime and chloramphenicol. Isolates from the late timepoint carried an additional Q176H substitution in AcrB (efflux pump). This resulted in an increase in MIC for both cefotaxime and chloramphenicol as well as tetracycline. Deletion and complementation of WT envZ had no effect on resistance while complementation with the R397H variant, reproduced the resistance results from the isolated strain. Deletion of*

1250 *acrB led to increased susceptibility against all efflux substrate antibiotics. Complementation*

1251 *with AcrB Q176K variant, in the ΔAcrB/ ΔRamR background, resulted in complete recovery*

1252 *of the resistant phenotype. **b,** q RT-PCR from 48-hour biofilms, using gyrB as a reference,*

1253 *resulted in significantly reduced ompF (large porin) expression, whereas ompC (narrow*

1254 *porin) expression significantly increased. **c,** Expression of csgA/B (main curli subunits) was*

1255 *abolished, explaining the pale morphotype cefotaxime-resistant-mutants exhibited. **d,** To test*

1256 *whether the changes on porin composition affect membrane permeability, drug accumulation*

1257 *was measured using the resazurin assay. A tolC::cat, pump-defective mutant, was used as a*

1258 *control. Both resistant mutants exhibited decreased drug accumulation, reflective of the*

1259 *altered membrane composition. **e,** Resistance against cefotaxime is a synergistic result of*

1260 *reduced membrane permeability due to porin alterations and increased efflux through the*

1261 *AcrA/B-TolC pump. **f,** Azithromycin exposed strains, from an early time point, obtained an*

1262 *AcrB R717L substitution which led to an 8-fold increase in azithromycin MIC. At a later*

1263 *stage, an additional substitution in RamR (T18P) emerged. This resulted in an MDR*

1264 *phenotype with increased MICs of azithromycin, chloramphenicol, nalidixic acid and*

1265 *tetracycline. Complementation of AcrB R717L in the ΔAcrB and of the RamR T18P in the*

1266 *ΔRamR background reproduced the resistance profiles of the strains isolated from the*

1267 *evolution experiments, confirming that these substitutions are responsible for the resistant*

1268 *phenotypes observed. **g,** Expression of acrB and ramA were monitored by q RT-PCR in 48-*

1269 *hour biofilms and showed increased expression of both acrB and ramA in the isolate*

1270 *carrying the RamR T18P substitution. **h,** Membrane permeability was monitored by the*

1271 *resazurin assay and reduced accumulation was observed because of the RamR T18P*

1272 *substitution, which potentially leads to overexpression of the RND pump. **i,** Resistance*

1273 *against azithromycin is a result of the modification of the AcrA/B-TolC pump, leading to*

1274 *increased efflux and overexpression of it due to the absence of negative regulation in the*

1275 *RamR T18P substitution strain.*

1276

57

1277
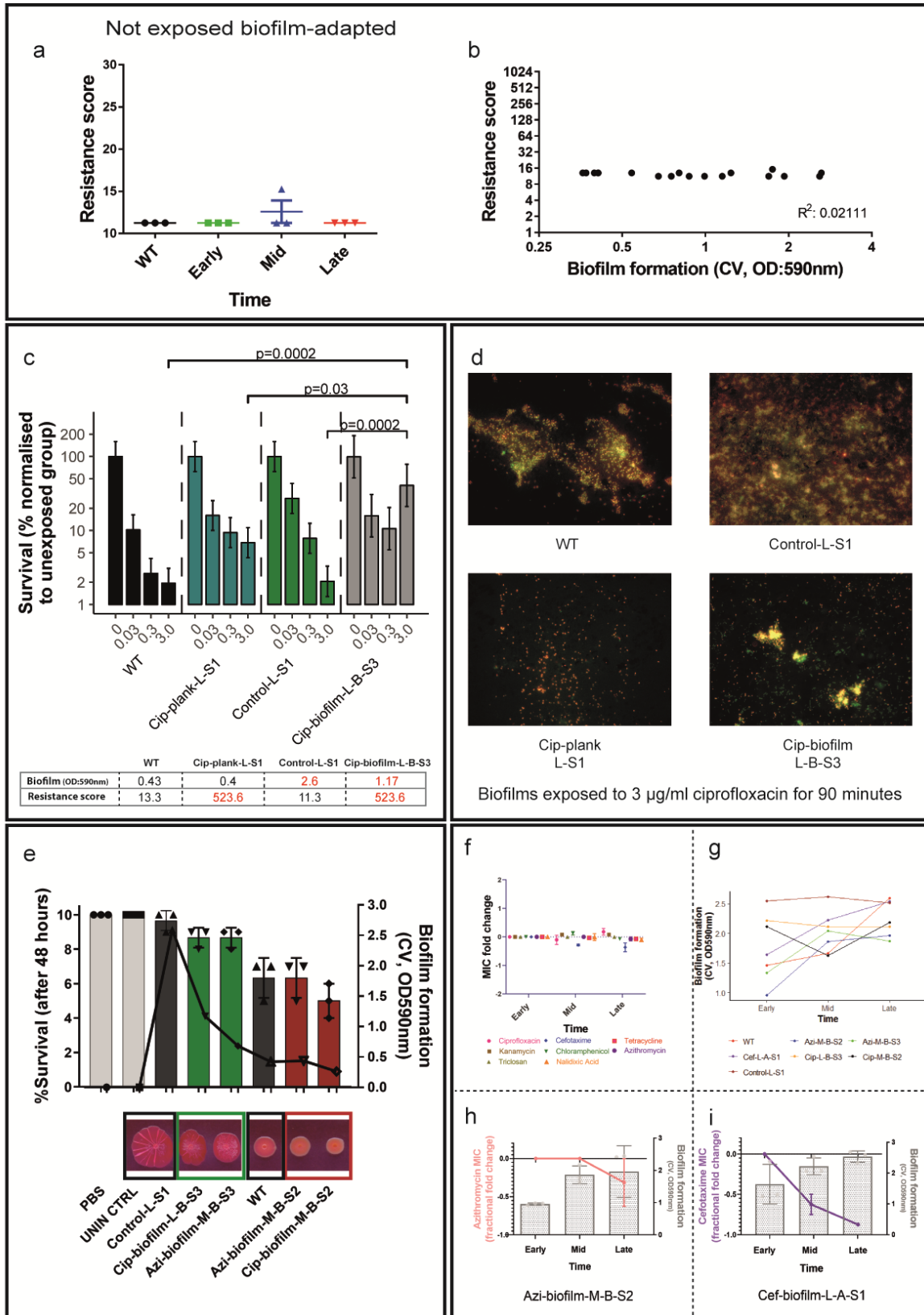
1278

Figure 6: Consequences of resistance. a, *Unexposed biofilm-adapted lineages were tested for resistance over time with no changes observed in their resistance score (additive value of*

1281   *all MICs determined for a strain). **b,** Although the strains adapted to forming better biofilms over*

1282   *time, their resistance score did not change. **c,** Biofilm viability was tested on 72-hour-biofilms grown*

1283   *on coverslips after treatment with increasing amounts of ciprofloxacin (0, 0.03, 0.3, 3 µg/mL). The*

1284   *strains tested were: cip-plank-L-S1 (resistant but low-biofilm former), control-L-S1 (not resistant but*

1285   *good biofilm former) and cip-biofilm-L-B-S3 (resistant and good biofilm former). Only biofilms*

1286   *produced by cip-biofilm-L-B-S3 were significantly harder to kill with ciprofloxacin. **d,** 72-hour-biofilms*

1287   *grown on coverslips were pre-treated with 3 µg/mL ciprofloxacin for 90 minutes, they were stained*

1288   *with live/dead stain and fluorescence microscopy was performed in a Zeiss Axio Imager M2. Different*

1289   *strains formed biofilms of variable density. An increased number of live cells was only observed in*

1290   *biofilms produced by the cip-biofilm-L-B-S3 strain, with surviving cells forming dense clusters on the*

1291   *coverslip. **e,** Pathogenicity (bars) was tested in the Galleria mellonella infection model. Each point*

1292   *indicates the average number of survivors from independent experiments and the bars show the*

1293   *average of these. The strains tested exhibited resistant phenotypes, with diverse biofilm abilities. WT*

1294   *and the unexposed control-L-S1 strain were used as a reference to the assay. Biofilm formation (lines)*

1295   *was measured by the CV assay and on CR plates. Survival was directly correlated with biofilm*

1296   *formation, with the weak biofilm formers causing more deaths in this model. **f,** Stability of resistance*

1297   *was measured by calculating the average of fold change in MIC per antibiotic, after ten 24-hour*

1298   *passages without any stressor present. For most antibiotics, resistance was stable throughout the*

1299   *accelerated evolution experiment except for cefotaxime. **g,** Biofilm formation increased significantly*

1300   *for the majority of the tested strains, by the end of the experiment. **h,** Individual example of an*

1301   *azithromycin resistant strain, which adapted and formed better biofilm over time without losing*

1302   *resistance to azithromycin. Pink line shows the changes in azithromycin MIC over time (line graph,*

1303   *left axis). Bars (bar chart, right axis) show the average biofilm formation from three replicates. Error*

1304   *bars indicate standard deviation **i,** Individual example of a cefotaxime resistant strain, which*

1305   *adapted to forming better biofilm but lost the resistance to cefotaxime. Purple line shows the*

1306   *changes in cefotaxime MIC over time (line graph, left axis). Bars and error bars are as above.*

1307 **Tables**

1308 **Table 1. Bacterial strains and vectors**

1309

Constructs/ Vectors	Source/ Reference	Description
pDOC-K	(60)	Gene doctoring deletion backbone
pACBSCE	(60)	Gene doctoring helper plasmid
pDOC-K/ acrB	Webber group	acrB deletion construct
pDOC-K/ ramR	Webber group	ramR deletion construct
pDOC-K/ yjcC	Webber group	yjcC deletion construct
pDOC-K/ envZ	Webber group	envZ deletion construct
pDOC-K/ glms	Webber group	Gene doctoring complementation backbone

pDOC-K/ glms/ *ramR*	Webber group	*ramR* complementation construct, under native promoter
pDOC-K/ glms/ *ramR* T18P	Webber group	*ramR* T18P complementation construct, under native promoter
pDOC-K/ *glms*/ *envZ*	Webber group	*envZ* complementation construct, under constitutive plac promoter
pDOC-K/ *glms*/ *envZ* R397H	Webber group	*envZ* R397H complementation construct, under constitutive plac promoter
pWKS30/ *acrB*	(61)	*acrB* complementation construct, under arabinose-inducible pbad promoter
pWKS30/ *acrB* Q176K	Webber group	*acrB*-Q176K complementation construct, under arabinose-inducible pbad promoter
pWKS30/ *acrB* R717L	Webber group	*acrB*-R717L complementation construct, under arabinose-inducible pbad promoter

Strains	Source/ Reference	Description
Salmonella enterica serovar Typhimurium (14028S)	(62)	Wild type strain
14028S/ Δ*acrB*	Webber group	*acrB* deletion strain
14028S/ Δ*ramR*	Webber group	*ramR* deletion strain
14028S/ Δ*envZ*	Webber group	*envZ* deletion strain
14028S/ Δ*acrB*/ p*acrB*	Webber group	*acrB* complementation strain
14028S/ Δ*acrB*/ p*acrB* R717L	Webber group	*acrB* R717L complementation strain
14028S/ Δr*amR*/ p*ramR*	Webber group	*ramR* complementation strain
14028S/ Δ*ramR*/ p*ramR* T18P	Webber group	*ramR* T18P complementation strain
14028S/ Δ*envZ*/ p*envZ*	Webber group	*envZ* complementation strain

14028S/ Δ*envZ*/ p*envZ* R397H	Webber group	*envZ* R397H complementation strain
14028S/ Δ*acrB*/ Δ*ramR*	Webber group	Double deletion strain
14028S/ Δ*acrB*/ Δ*ramR*/ p*acrB*	Webber group	Double deletion strain/ *acrB* complementation
14028S/ Δ*acrB*/ Δ*ramR*/ p*acrB* (R717L)	Webber group	Double deletion strain/ *acrB* complementation-SNP variation

1310

1311 **Table 2. Primers used in this study**

Name	Sequence	Use
AcrB-part1 for (EcoRI)	TACGTGAATTCCACGCGGCGATGCCACGGTG	*acrB* deletion
AcrB-part1 Rev (BamHI)	GCATAGGATCCAAATATAGGGCGATCGATAA	*acrB* deletion
AcrB-part2 for (XhoI)	TACGTCTCGAGATTGAGCATAGTCATTCGAC	*acrB* deletion

AcrB-part2 Rev (NheI)	GCATAGCTAGCGTTTGTGTAATCATTGGGTT	*acrB* deletion
RamR part1-For (EcoRI)	TACGTGAATTCAAACTCGTCAGCGGCTCCCG	*ramR* deletion
RamR-part1 Rev (BamHI)	GCATAGGATCCTTTTTTGTCTTCACTCTTCG	*ramR* deletion
RamR-part2 for (XhoI)	TACGTCTCGAGTGGCGCGCGCTGACTCGCGA	*ramR* deletion
RamR-part2 Rev (NheI)	GCATAGCTAGCTATCCTCGCCCGCATAGACT	*ramR* deletion
*EnvZ*_part1_For (EcoRI)	TACGTGAATTCCGCGAGATGTTC	*envZ* deletion
*EnvZ*_part1_Rev (BamHI)	GGATCCGGATCCAACTTCGC	*envZ* deletion
*EnvZ*_part2_For (XhoI)	TACGTCTCGAGCGCGTCCAG	*envZ* deletion

*EnvZ*_part2_Rev (SpeI)	AGTACTAGTGCTGTTCGATCTGGCGATCCCGAC	*envZ* deletion
*Glms*_part1_For (EcoRI)	TACGTGAATTCGCTCGAAGGCGCGCTGAAG	pDOC-K/*glms* generation
*Glms*_part1_Rev (KpnI)	ACGTAGGTACCCGGCCTTCTGCCTGGTACTACATTTG	pDOC-K/*glms* generation
*Glms*_part2_for (XhoI)-MCS	TACGTCTCGAGCATATGCCCGGGGCGGCCGCAAGCTTTCGACAGACGGCCTTTTTTTG	pDOC-K/*glms* generation
*Glms*_part2_Rev (NheI)	GCATAGCTAGCCGGTCAATTTCCCCATTCCC	pDOC-K/*glms* generation
RamR-compl-For (XhoI)	GCATACTCGAGTTCATGCGGCAGCCCTTG	*ramR* complementation
RamR-compl-Rev (HindIII)	ACGTAAAGCTTTTATTGCTCCTCGCGAGTCAGC	*ramR* complementation

EnvZ-compl-For (XhoI)	ATCACTCTCGAGTTTACACTTTATGCTTCCGGCTCGTATGTTGCAGACCGTCTGGG GCCTGG	*envZ* complementation
EnvZ-compl-Rev (HindIII)	GGACGTAAGCTTTTATGCCTCTTTTGTCGTCCCCTGGAC	*envZ* complementation
GyrB-RT-For	GGAAGGGGACTCCGCGGGCG	q-RT PCR
GyrB-RT-Rev	CAGCGGCGGCTGCGCAATGT	q-RT PCR
RamA-RT-For	CGCTCAGGTTATCGACACGA	q-RT PCR
RamA-RT-Rev	CCACTTGGAATACCCCGCAT	q-RT PCR
OmpF-RT-For	GGCGGCGCCTATACTGATAA	q-RT PCR
OmpF-RT-Rev	CGAAAGAGAGACCGTCCACC	q-RT PCR
OmpC-RT-For	TTATGCAATCGGCGAAGGCT	q-RT PCR
OmpC-RT-Rev	GTTACCATACAGGCGAGCGT	q-RT PCR
CsgA-RT-For	CATCGACCAGTGGAACGCTA	q-RT PCR
CsgA-RT-Rev	TACGCTGGAATCAGATGCGG	q-RT PCR
CsgB-RT-For	TGCAACCGCGACAAATTATGA	q-RT PCR

| *CsgB*-RT-Rev | TTGACCAATAATGGCCGCCT | q-RT PCR |

1312